Graphene transfer process based on gels.

Master's thesis

University of Jyväskylä

Department of Chemistry

24.04.2023

Santeri Neuvonen

Abstract

In this thesis, we suggest an alternative approach to graphene transfer by using gel materials as a support layer. The literature section focuses on graphene and its properties to find the optimal gel for the graphene transfer process. The experimental section focuses on establishing a working gel transfer for the graphene by experimenting with hyaluronic acid, N-fluorenylmethoxycarbonyl phenylalanine (Fmoc-F) and dipeptide tert-butyloxycarbonyl diphenylalanine tert butyl ester (BocFFOtBu) gels.

The experiments did not produce an efficient amount of transferred graphene to be used in graphene devices. However, the result demonstrated that the required interactions between graphene and gels are sufficient enough for the transfer, therefore the proposed method needs to be optimized and studied further.

Prologue

This master thesis and research project were done at the Department of Chemistry and the Nanoscience Center at the University of Jyväskylä. The thesis and research project was done during 2022. The project was performed mainly in the Nanoscience Center cleanroom and at the atomic force microscope laboratory. In addition, the Raman spectrometer at the Department of Chemistry was used in the project. Data processing softwares used in this thesis were Gwyddion, Brukkers Nanoscope analysis, Origin, and custom-made Raman MapViewer software. Literature research was mainly done by using google scholar and JYK.doc services. Supervision of the work was done by senior researcher Andreas Johansson and postdoctoral researcher Sitsanidis Efstratios.

I would like to thank Andreas Johansson for his great guidance during the thesis and for the opportunity to work on an interesting project. I would also like to thank Sitsanidis Efstratios for the excellent guidance and teaching in the field of gels. Both instructors gave excellent feedback during the writing process. I would like to thank laboratory technician Olli Rissanen, who prepared the high-quality graphene samples for the experiments. I would also like to acknowledge the computational resources from FGCI (Finnish Grid and Cloud Initiative) and thank Laura Laverdure for guidance and assistance in the computational section of the thesis.

Jyväskylä 24.04.2023
Santeri Neuvonen

Contents

Abbreviations and terms

Abbreviation	**Meaning**
GO	Graphene oxide
rGO	Reduced graphene oxide
fGO	Functionalized graphene oxide
CVD	Chemical vapor deposition
$\alpha Al_2O_3(001)$	Alpha aluminium oxide
PMMA	Poly(methyl methacrylate)
AFM	Atomic force microscope
STM	Scanning tunnelling microscope
gel-sol transition	Transition of the gelator to a solid gel
AR-PPG	Acid resistant preformed particle gels
ECM	Extracellular matrix
G+	Gram-positive
G−	Gram-negative
HA	Hyaluronic acid
EDCI	1-(3-Dimethylaminopropyl)-3-ethylcarbondiimide hydrochloride
ADH	Adipic dihydrazide
Fmoc-F-OH	*N*-[(9H-Fluoren-9-ylmethoxy)-carbonyl]-L-phenylalanine
BocFFOtBu	*N*-tert-butyloxycarbonyl (Boc)–L-phenylalanyl–L-phenylalanine tert-butyl ester
tBuOAc	tert-butyl acetate

1 Introduction

Graphene is potentially one of the most versatile future materials in nanotechnology. It has been used for applications in electronic circuits, the development of new generation sensor technologies, biological sensors or in combination with computers and biological systems.[1,2,3] Graphene is produced in multiple ways, which are constantly being developed further while the race for ultra-clean graphene is on.

Graphene was first created by mechanical exfoliation but at the moment, the most common way to synthesize graphene is chemical vapour deposition (CVD), in which graphene is formed on a catalytic surface using high pressure and temperature. Common phases of graphene synthesis consists of annealing the catalytic surface, the formation of graphene, and the cooling of the sample.[1,4] However, graphene production has not yet reached the industrial scale of use because the current method creates a lot of contaminates and residues on its surface. For this reason, researchers are trying to find alternative methods to produce clean graphene by replacing the transfer polymers with other polymers or even with different materials, such as gels.[5,6]

The challenge in graphene transfer with polymers is the contamination that is left on graphene after transfer. These contaminants are polymer residues that are not removed by dilution or annealing. The scientific community has presented multiple different ways to approach this problem and attempts to solve it have been well documented. Different cleaning methods for the polymer surface have been proposed and their results vary.[7] Another popular approach for solving this problem is to test a new transfer polymer. This introduces new cleaning procedures.[5] Despite the efforts of the scientific community, a reliable method for graphene transfer that would create ultra-clean graphene has not yet been realized.

In this thesis, we propose an alternative approach to the graphene transfer process by changing the graphene support polymer to a self-supporting gel. Graphene monolayer is able to induce interactions with multiple different surfaces and materials[5,6,8], thus making the transfer with a gel layer a possible option by graphene qualities alone.[9] Graphene has been transferred with the help of a gel layer[10], where the gel functioned as a "glue" between graphene monolayer and the support material. Our aim is to achieve graphene transfer with only gel, without additional support layers, and to remove the gel with

minimal residues. During the time period of this thesis work, no other research group has reported any studies or research results related to gel-based graphene transfer.

Using gel as a graphene transfer support layer opens new windows to many practical applications. Gels could be easily removed from graphene by heating, dilution, or enzymatic reactions.[11,12,13] The latter of the removal methods could have a plethora of applications in biological systems, such as drug delivery, tissue healing, or bio-sensory. Gel assisted transfer could be applied in industrial scale for the mass production of graphene in reliable and environmentally friendly processes. Physiologically decaying gels could be the key to a new generation of biotechnology, such as sensors or prosthetic limbs.

2 Properties of graphene

Graphene is a two-dimensional crystal with a hexagonal honeycomb structure made of carbon atoms.[1,14] Each atom is bonded to three neighboring atoms by strong σ-bonds at a 120^o angles. The structure of graphene is shown in Figure 1. The bonding is due to the hybridization of the carbon's atomic orbitals (2s, $2p_x$ and $2p_y$). This leaves the unbounded valence electron in the $2p_z$ orbital, which is orthogonal to the graphene plane. The orthogonal bonding to graphene occurs with this orbital. The $2p_z$ orbitals also add to the electronic transporting properties of graphene, where the delocalized π electrons overlap and form weaker bonds.[1,9]

Graphene was first isolated in 2004 by Novoselov *et al* .[1] by mechanical exfoliation, by which they were able to repeatedly peel off small graphene sheets from a few layers of graphite. Indeed, they were able to remove up to 15 μm large single-layer graphene films from a sheet of graphite. The method was repeatable and reliable, though very time and work-intensive. The single-layer graphene films showed excellent conductive and mechanical properties compared to graphite. Its unique properties can be explained using a model for 2D metal with band overlapping ($\delta\varepsilon$) between valence and conductance bands. The band overlap of graphene and graphite varies depending on the number of layers. This means that graphene is comparable to a sheet of metal conductor and could be used in multiple different electrical component applications, for example in transistors.[1]

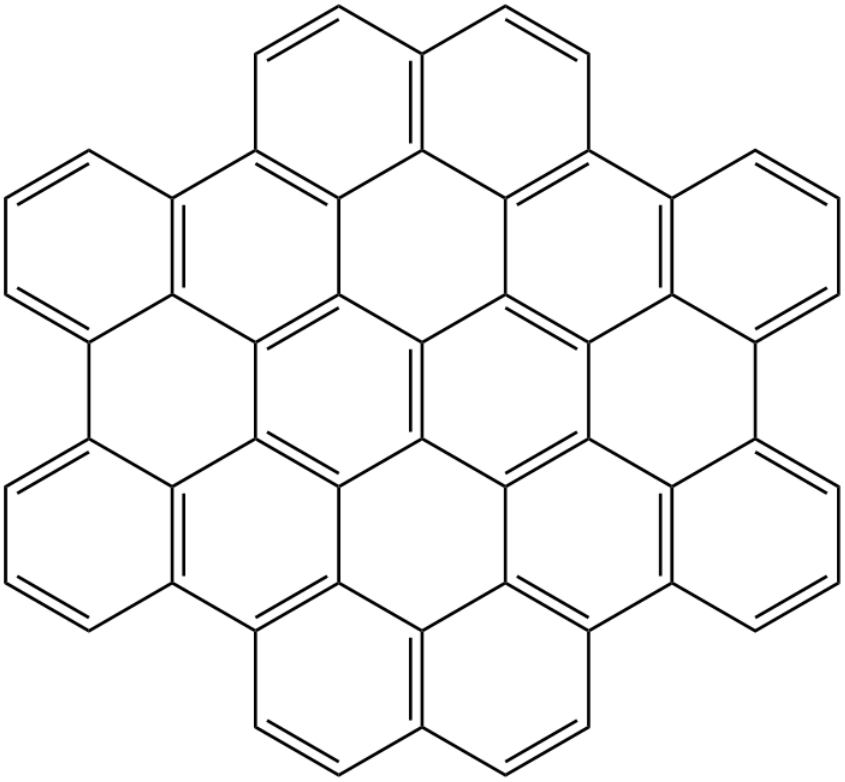

Figure 1: Molecular structure of graphene.[1,14]

Analyzing graphene at a quantum mechanical level, the wave function of graphene is formed as follows:

$$\Phi_A = \frac{1}{\sqrt{N}} \sum_{R_A} e^{ikR_A} \varphi(r - R_A) \tag{1}$$

where N is the number of unit cells, which in the case of graphene, consists of two bonded atoms, R_A is the position of the atom and $\varphi(r\text{-}R_A)$ is the atom's $2p_z$ orbital. The sum in the equation runs over all possible lattice vectors of the unit cell.[9]

The mechanical properties of graphene are stunning for its size. Graphene has Young's modulus between 0.5-1.0 TPa, which is significantly greater than many other 2D materials. Graphene also has a tension of hundreds of nano-Newtons,[15,16] is hydrophobic and very stable. Even though graphene is stable in high temperatures, its reactivity changes by temperature variation. At lower temperatures, graphene tends to spontaneously reduce and at higher temperatures, it tends to oxidize. At atmospheric pressure and room temperature, graphene favors reduction, but already at around 27 ℃, graphene starts to oxidize.[17]

Graphene is well known for its extraordinary electronic transport properties. This has led graphene to be used in electronics for different applications. Graphene transistors are

an excellent example of such use. Using graphene in circuits can be challenging. Indeed, at graphene and metal junctions a notable charge transfer occurs. This causes a local band-bending, because of the doping of graphene. This problem is overcome by using charge carrier molecules to minimize charge transfer stress on the graphene. Transistors work, for example, by injecting carrier molecules on top of graphene while a gate-induced electric field is used to control the transport voltage.[2]

Graphene has also great optical properties, that can be tuned in a wide range of wavelengths. As these include visible light, graphene can be used in optical detectors and other photo-electronics. Exited states of graphene decay quickly, in the matter on picoseconds. This speed is affected by the doping of graphene. When field gradients are introduced to the photoexcitation of graphene, graphene starts to produce photocurrent. This can be used in optoelectronic applications. As with the transistors, metal-graphene interactions in optoelectrical processes produce doping and therefore band-bending, but in these applications, this can be used to increase the photodetection of the system. Graphene's sensitivity to light in a wide range of wavelengths can also be used in conjunction with its saturated absorption. This ability can be used in lasers to produce very short, up to picosecond, laser pulses.[2] Graphene's optical properties also allow its shaping by high-intensity lasers. 2D graphene can be forged into 3D structures like multi-layer pyramids. This is achieved using a femtosecond laser under an inert atmosphere. This method alternates the graphene's structure, thus it can be detected by optical microscopy much easier than regular graphene..[18]

The symmetry properties of graphene can be analyzed using the known symmetry and character table (seen in Table 1).[19,20] Graphene has a two-dimensional lattice and it has a six-fold rotation axis and a horizontal reflection symmetry plane. When using regular definitions to molecular symmetry, graphene has the point group D_{6h}.

Derivatives of graphene are usually made by oxidizing or reducing graphene. The most common graphene derivative is graphene oxide (GO). Oxygen atoms that attach on the surface of graphene create functionalized active positions where desired atoms or molecules can later be chemically attached. GO and other derivatives are easy to create thanks to the "quick" oxidization tendency of graphene. Graphene starts to oxidize in very small temperature increments starting from the average room temperature in ambient air.[17] Graphene derivatives can also be created by changing the pH. Treatment of graphene in

basic pH (above 7) and oxidizing reagents cause graphene to oxidize and form GO. GO can then be processed even further using different pH values. If the desired final product is reduced graphene oxide (rGO), the GO is placed in an acidic solution (pH below 7). If the final product is functionalized graphene oxide (fGO) the GO is placed in a basic solution to endorse further oxidation. The structural differences of these derivatives and the effect of pH on the structure are shown in Figure 2.[21]

Table 1: Point group of graphene (D_{6h}).[20]

$\mathbf{D}_{6h}$	E	$2C_6$	$2C_3$	C_2	$3C_2$'	$3C_2$"	i	$2S_3$	$2S_6$	σ_h	$3\sigma_d$	$3\sigma_v$		
A_{1g}	1	1	1	1	1	1	1	1	1	1	1	1		x^2+y^2, z^2
A_{2g}	1	1	1	1	-1	-1	1	1	1	1	-1	-1	R_z	
B_{1g}	1	-1	1	-1	1	-1	1	-1	1	-1	1	-1		
B_{2g}	1	-1	1	-1	-1	1	1	-1	1	-1	-1	1		
E_{1g}	2	1	-1	-2	0	0	2	1	-1	-2	0	0	(R_x,R_y)	(xz, yz)
E_{2g}	2	-1	-1	2	0	0	2	-1	-1	2	0	0		(x^2-y^2, xy)
A_{1u}	1	1	1	1	1	1	-1	-1	-1	-1	-1	-1		
A_{2u}	1	1	1	1	-1	-1	-1	-1	-1	-1	1	1	z	
B_{1u}	1	-1	1	-1	1	-1	-1	1	-1	1	-1	1		
B_{2u}	1	-1	1	-1	-1	1	-1	1	-1	1	1	-1		
E_{1u}	2	-1	-1	-2	0	0	-2	-1	1	2	0	0	(x,y)	
E_{2u}	2	-1	-1	2	0	0	-2	1	1	-2	0	0		

For biological applications, graphene can be applied in several different ways, such as drug delivery.[3,8,10] The unique bonding applications allow graphene to work as an immobilizer of proteins and enzymes. Graphene-immobilized enzymes possess higher storage and thermal stability. Therefore, multiple application opportunities in sensors, catalysis, and biotechnology fields are available. Binding of enzymes and proteins is a great example of the graphene surface qualities, as there are multiple ways for the molecules to attach to the surface. The non-covalent interaction between enzymes and graphene can be achieved without any catalyzing substances. The bonding depends on the status of the active functional groups in the enzyme, the environment's acidity, and temperature. The strongest interaction with graphene is formed by hydrophobic enzymes. Theoretical calculations have shown that the key feature in the bonding is π-π stacking that occurs be-

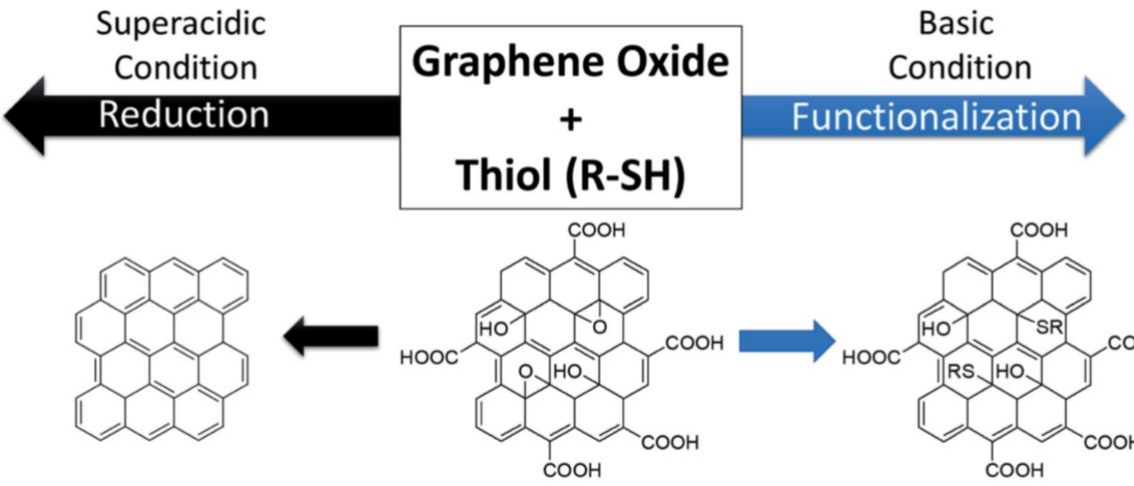

Figure 2: Effect of pH change to GO structure and creation of rGO and fGO. Adapted with permission from De Leon, A., Mellon, M., Mangadlao, J., Advincula, R. and Pentzer, E., The pH dependent reactions of graphene oxide with small molecule thiols, RSC Advances, 2018, 8, 18388–18395.[21]

tween graphene and enzyme. Covalent bonding of the enzymes can happen spontaneously or via the use of linking molecules. Linking molecules can attach to graphene by chemical bonding or physical interactions such as π-π stacking. In both cases, the enzyme immobilization does not affect the morphology of graphene. Immobilizing enzymes and proteins can improve graphene biocompatibility. Though graphene is not a toxic organic material, it is still a foreign substance that is not found in the human body naturally. Enzymes could be used to induce many biological processes and the degeneration of graphene. The immobilized enzymes could assist in the degeneration of graphene when it is no longer needed. This way it does not stay in the body.[8]

The study of enzyme, protein, and peptide immobilization opens doors for many different applications in organic, inorganic, and industrial fields for the use of graphene and functionalized molecules. Functionalized molecules can be used to create new-generation materials or as docking materials in different sensors and assembly sites. Graphene can absorb peptides on its surface with electrostatic or π-π stacking. Peptides could be used in conjunction with graphene as sensors to identify small molecules. There is a possible application to use a peptide-graphene sheets as construction platforms for complicated nanoparticles and multifunctional structures.[8]

2.1 Graphene synthesis on copper

2.1.1 Graphene growth process at the Nanoscience Center

The growth of graphene was done at the Nanoscience Center at the University of Jyväskylä, by an adaptation of the method described in the article "Giant secondary grain growth in Cu films on sapphire" by David L. Miller.[4] Copper was vaporized to crystalline $\alpha Al_2O_3(001)$ which had been cut to small wafers of 50 mm by 50 mm and annealed in a furnace with atmospheric pressure oxygen at 1100℃ for 24 hours. This process removes scratches and potential contaminants from the top surface of the sapphire wafers. The wavers were then placed at Cu puck which was transferred in a vacuum sputter deposition system. 99,999 % of pure Cu was vaporized on the surface of the sapphire, forming 450 nm copper layer, which was deposited at a rate of 1 nm/s. The copper had a Cu(111) orientation. Films that had deposition temperature below 500 ℃ were deposited using a load-locked, turbo-pumped chamber, which had a base pressure of $2*10^{-9}$ mbar, from a distance of 8 cm and a sputtering power of 100W in $1,7*10^{-3}$ mbar of argon (Ar). Films that had deposition temperature equal to or above 500 ℃ were deposited in a cryo-pumped bell-jar-style chamber, that had a base pressure of $2*10^{-7}$ mbar, from a distance of 10 cm and a sputtering power of 200W in $6,7*10^{-3}$ Pa of Ar. After deposition, each waver was coated with PMMA and diced thereafter to 5x6 mm chips. The PMMA was cleaned from the top of the samples using ultrasonic agitation in acetone and isopropanol before annealing and characterization. Annealing was performed at a base pressure of $6,7*10^{-3}$ between temperatures of 950-1050℃ for 40 minutes in a hot-wall tube furnace. To limit the Cu sublimation, the pressure was kept at 53 mbar during the synthesis of graphene. The annealing was performed by flowing 500 sccm of 99,999% pure Ar and 11 sccm of 0,2% hydrogen gas (H_2) in Ar. The H_2 partial pressure was around $23*10^{-4}$ mbar.

The graphene growth occurred at 1055℃ in 40 minutes. The growth began when 14 sccm of 0,2% methane gas (CH_4) was introduced to the furnace. During the growth, the CH_4 partial pressure was around $28*10^{-4}$ mbar. When a monolayer of graphene had been synthesized, it was taken out of the furnace and prepared for the transfer process. The graphene/Cu chip was spin-coated with PMMA and bagged at 150 ℃. After bagging, thermal release tape was applied on top of PMMA. The chip was floated

at the surface of ammonium persulfate ($(NH_4)_2SO_8$). The chip was left to float overnight to etch the Cu layer away. When the Cu had been etched away, the Al_2O_3 substrate sunk to the bottom of the flask, and the graphene/PMMA/tape floated on the surface. The graphene/PMMA/tape layer was rinsed with deionized (DI) water and placed on top of 9x9 mm silicone oxide (SiO_2) chip. To release the thermal release tape, the chip was heated to 150 ℃ and then to 180 ℃ to soften the PMMA layer and to enhance the graphene bond towards SiO_2. Finally, the chips were submerged in glacial acetic acid (CH_3COOH) for several hours at room temperature to remove the PMMA layer.[4]

During the graphene synthesis, there is a possibility for defect formation. Graphene defects refer to an abnormality in the graphene crystal structure (Figure 1). In addition to structure, defects affect the conductivity and reactivity of graphene. Defects occur between a few atoms and are not stationary. The defects can move slightly or can change position in the structure. The defects can be caused by foreign atoms on the graphene or copper surface during the synthesis. These are extrinsic defects. If the defect is formed without an external manipulator, it is known as an intrinsic defect. The simplest example is the point defect, where one carbon atom is missing, resulting in a 5-carbon ring instead of 6. This defect is more common in synthetic methods that operate below 1000 ℃. The simplest defects are the single vacancies, where two of the three bonds that would attach to the carbon are saturated and the carbon atom doesn't have a stable position to bond. Thus, the crystal structure is missing one carbon atom. This defect creates penta- and nona- carbon rings in the structure. Multiple vacancies are formed when multiple carbon atoms are not able to bond due to bond saturation. The form of the defect depends on the number of carbon atoms missing from the structure. For example, missing two carbon atoms forms two pentagons and two octagons in the crystal structure. Missing more than two atoms creates more complex structures in the lattice. The absence of an even number of carbon atoms is more common, as being energetically more favorable and easier to fix naturally than the absence of an odd number of atoms.[22]

The defects in the graphene structure can also be three dimensional. These defects form during the synthesis process due to the excess of carbon. Carbon adatoms, atoms that don't fit to the crystal structure, attach on top of C-C bonds and use the free π-orbitals of the carbons to bond to the structure. The bonding carbons are sp^3 hybridized and form covalent bonds with the excess carbon atoms. These defects are mobile, and the

migration of the atom can occur rapidly. The moving adatoms can meet each other on the graphene surface and react. This forms two sp^2 hybridized atoms that can attach to the graphene structure causing a more stable defect in the structure. This can also happen with foreign adatoms, that attach to graphene from air. The severity of the defect depends on the adatoms' interaction with graphene. If the adatom does not interact strongly with graphene, the resulting defect has an insignificant effect, as the adatom attaches only via Van der Waals forces. A stronger adatom can attach itself to any position on top of graphene. Strongly interacting adatoms can bond to reactive sites on graphene or the attached molecules and alter the structure, preventing or causing reactions.[22] The reaction follows the equation:

$$\mathrm{XCH_4(g)} \xrightarrow{\mathrm{Cu}} \mathrm{C_X(s)} + 2\,\mathrm{H_2(g)} \tag{R1}$$

in which X refers to the amount of reacting methane.

3 Characterization methods

To evaluate the quality of graphene, different techniques can be applied to assess its properties and potential contaminants on its surface.

3.1 Raman spectroscopy

Raman spectroscopy is one of the best methods to analyze graphene as it is non-invasive, offering a safe nondestructive analysis of graphene samples.[23] Raman spectroscopy is named after the Indian scientist C.V. Raman, who was the first to observe the scattering in 1928.[24] Raman spectroscopy measures the scattering of electromagnetic radiation from the sample molecules. The scattering effect is produced from an oscillating induced dipole. Samples can scatter electromagnetic radiation by increasing or decreasing the energy of the radiation. This is called the Raman effect. The direction in which the shift occurs is called Stokes-Raman scattering, if the energy increases, and anti-Stokes, if the energy decreases. As Raman scattering is relatively weak, the radiation should be intense and

monochromatic.[24,25,26] The frequency shift in Raman spectroscopy can be a result of transitions between the molecular energy levels, rotational, vibrational or electronic. Due to these varieties, all the scattering of incident frequency, Stokes and anti-Stokes scattering regions can be observed in the same spectrum.[24]

Raman scattering can also resonate. This can be taken advantage of in resonance Raman spectroscopy. Resonance Raman spectroscopy can be detected when the energy of the exciting radiation is close to the manifold of the exited state.[26]

In the case of graphene, the three most interesting peaks are the D, 2D, and G bands. Different shapes and shifts of these bands reveal details regarding the layers and potential contamination of the samples.[23] Graphene belongs to the D_{6h} point group and from the reducible presentation and the rotational and transitional mode knowledge (symmetry table 1) the vibrational mode representation can be obtained. The vibrational mode representation is:[19,23]

$$\Gamma^{vib} = A_{2u} + B_{2g} + E_{1u} + E_{2g}$$

Graphene has six normal modes, of which two are doubly degenerative. From the presentation and the character table (Table 1), certain observations can be made. For instance, the only vibrational mode, which is only Raman active and doesn't have infrared mode, is E_{2g}. This is referred to as the degenerate in-plane optical mode, however, the out-of-plane optical mode B_{2g}, is neither infrared nor Raman active.[23]

The spectrum abides by the Raman selection rules. This can be observed in the activation of the one-phonon modes. One-phonon modes of graphene symmetry (when the symmetry vectors are equal to zero) can only be active when there is no contamination. From the graphene spectrum, only the D and G bands of the spectrum meet these requirements. The G-band represents the high-frequency E_{2g} mode phonon and the D-band the breathing mode of the six-atom carbon rings. The latter is activated by interactions with the rings' π orbitals, thus the peak is more visible in graphite and in cases of contamination on top of the ring. The decay rate of the intermediate states is determined by their population. The decay rates for either the unpopulated π^* or populated π bands are given by the scattering rates of electrons.[23] When multiple layers are present, there are

more intermediate states present, meaning that distorting signals occur. This leads to a shift in the low wavenumber region, especially in the G band. An example of Raman spectra of pristine and contaminant graphene is given in figure 3.[27]

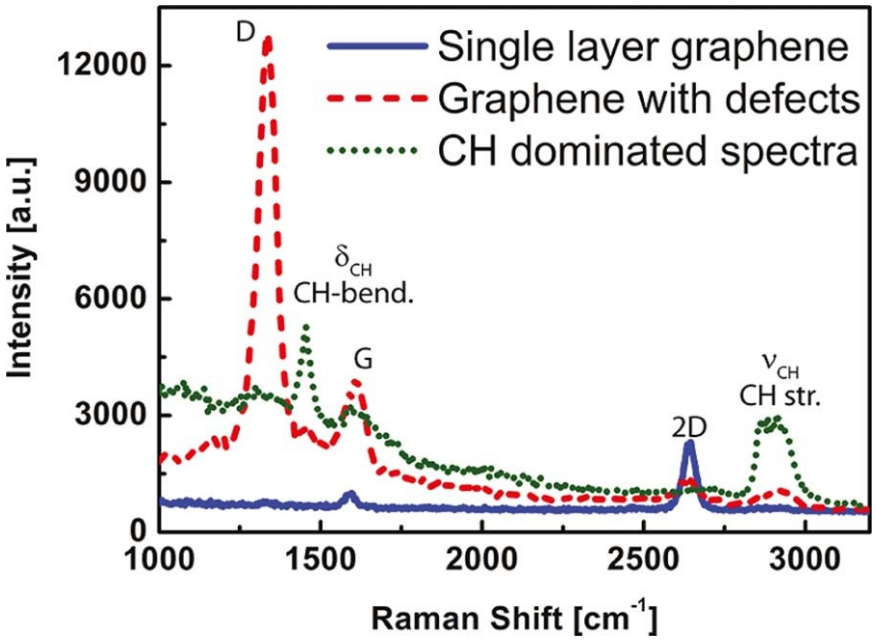

Figure 3: Raman spectra of single layer pristine graphene (blue), defected graphene (red) and contaminant graphene (green). Adapted with permission from Nanda, S. S., Kim, M. J., Yeom, K. S., An, S. S. A., Ju, H. and Yi, D. K., Raman spectrum of graphene with its versatile future perspectives, TrAC - Trends in Analytical Chemistry, 2016, 80, 125–131.[27]

3.2 Atomic force microscopy

Atomic force microscopy (AFM) is based on the scanning of the sample's surface with a probe head, at near-touch distances. AFM creates a map of the topographic and height information of the sample. Compared to other methods, which study the topography of materials, AFM can produce the most precise data than scanning tunneling microscopy (STM), for example, as it has a sharper analyzing tool, finer control over the probe-surface forces, and stronger feedback. One of the strengths of AFM is the non-invasive sample preparation process in contrast to other analytical methods such as scanning electron microscopy (SEM) and transmission electron microscopy (TEM). AFM was developed in 1986 by Gerd Binnig, Calvin Forrest Quate, and Heinrich Rohrer.[28]

The function of AFM is based on piezoelectric transducers, force transducers, and the feedback control. Piezoelectric transducers are electromechanical transducers that convert the electric potential to mechanical motion. Piezoelectric materials are used for the precise control of the AFM while scanning the sample. The force transducer measures the force between the sample's surface and the AFM probe. The force transducer can be tuned to sense forces as small as 10 pN, making even the smallest changes visible in otherwise monotonic data. The most common force transducer on AFM is a cantilever with an integrated tip, but there are other types of force sensors that can also be applied. The feedback control is the key element in the resolution of AFM, as the constant feedback from the sensors allows the correct amount of force to be applied on the surface to create as precise data as possible. To achieve this, the sensitivity of piezoelectrics is used to quickly react to the data produced by the force transducer, keeping the measuring force at a desired level.[28a]

An AFM sensor is an optical cantilever, on which a laser beam is pointed at. The laser beam reflects from the cantilever to a four-segment photodetector. When the probe interacts with something on the surface of the sample, the position of the laser changes in the grid. The AFM data are produced based on changes as such. This method is precise since small changes to the laser alignment cause great changes in the data.[28b] The structural components of an AFM apparatus is presented in figure 4.[29]

AFM can produce high-resolution images that range from a sub-millimeter to nanometer scale and it produces a three-dimensional profile of the image. AFM can also be used to study liquids or highly viscous samples. The range of data is not confirmed solely to just topographic data. Other known properties of the cantilever and the microscope can be used to obtain detailed data than just a height profile. AFM can be used to measure, for example, adhesion (vide infra section 3.2.2 and experimental section).[30]

3.2.1 Gel characterization

AFM imaging is an excellent method for the study of gels. One of its advantages is the absence of pre-measurement sample treatment, meaning that the gels can be studied with no manipulation or added materials in their structure. However, the challenge in AFM imaging is that the tip could apply excess force on the gel structure and flatten it much

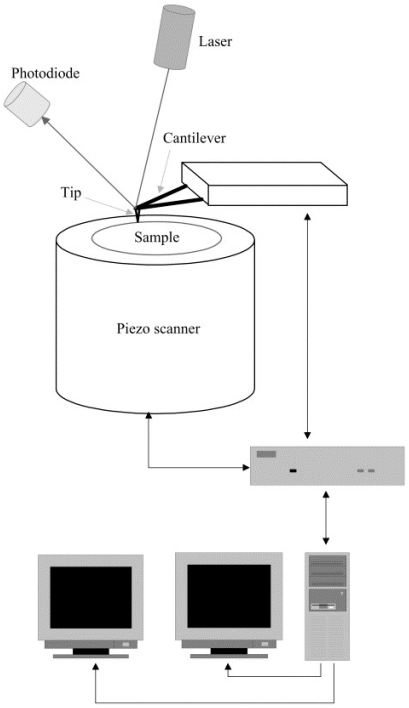

Figure 4: Schematic representation of the components of the atomic force microscope. Adapted with permission from Santos, N. C. and Castanho, M. A., An overview of the biophysical applications of atomic force microscopy, Biophysical Chemistry, 2004, 107, 133–149.[29]

easier than with harder materials. This distorts imaging making the structure look wider and possibly even causing damage to the soft material's surface.[30]

AFM, as a supplementary method, may be used to study the interactions between the molecules in the gel, in addition to spectroscopy analysis. Especially, the intermolecular interactions and the physical bonding, like π-π and hydrogen bonding of the gelators reveal important information about the self-assembly process. The AFM helps to study the charge transfer interactions in π-π interactions, where one of the functional groups of the gelator acts as a donor and the other as an acceptor of electrons. If the acceptor-donor interaction is strong enough, the two molecules would react or form a covalent bond.[30]

Rao *et al.*[31] reported the use of AFM to study the self-assembly of a charge-transfer complex in a hydrogel. The group demonstrated a directional self-assembly process in supramolecular charge transfer that led to directional π-π stacking of the gelators. They reported the use of AFM to image the formed gel and to deduce the arrangement of the formed micelles. The AFM analysis enabled the identification of the donor and acceptor

within the gel structure and enhance the understanding of the self-assembly process in the studied system.[30,31]

3.2.2 Adhesion

While studying graphene, with AFM, one of the key information refers to adhesion. Adhesion reveals the bonding effects between two solid materials and how much stress the molecular bonds are able to sustain or transmit. Adhesion can be formed by Van der Waals forces, hydrogen bonds, mechanical interlocking, or electrostatic interactions.[32,33a] The strength of adhesion can be tested using a peel or shear test as a convenient practical method. These tests can determine the energy dissipation associated with the bulk deformation of the adhesive and the adherents as well as the contribution of interfacial forces. The practical strength of the adhesion bond depends on a variety of factors like geometry, bonding rate, temperature and the mechanics of the measurement method.[33]

The adhesion energy between graphene and SiO_2 is reported to be approximately 0.46 Jm^{-2} and between graphene and Cu 0.75 Jm^{-2}.[34] Using adhesion energies, Das *et al.*[35] was able to calculate the bonding strength between graphene and Cu. The energy was calculated to be approximately 12.75 Jm^{-2}. The adhesion energy (γ) of a 2D material can be calculated by equation 3:[36]

$$\gamma = \lambda E h (\frac{\omega}{a})^4 \tag{2}$$

where λ is the geometrical factor, E is the elastic modulus of the material, h is the thickness, ω is the central blister displacement and a is the radius of the analyzed material. However, this equation considers various conditions to be applied to graphene materials. Since graphene is flexible, the dominant deformation mode is stretching. This leads to the case, where ω»h and a»h, which in classical cases is opposite to the true relations. The effect of inter-surface potential is assumed to be minimal and only effective during contact or close interface. The truth is that there is a finite range for Van der Waals, electrostatic, and meniscus force effects. Finally, the substrate is presumed to be stiff and the change in the formation should not affect the qualities of the substrate. Due to the properties of graphene, these assumptions can be justified and equation 3 can be used.[36]

The surface and interfacial properties determine the thermodynamic work of the adhesion forces, W. Equation 4 gives W between two different surfaces in contact:[33a]

$$W = \gamma_1 + \gamma_2 - \gamma_{12} \tag{3}$$

where γ_1 and γ_2 are the surface energies of materials 1 and 2 and γ_{12} is the interfacial energy between them. The practical strength of the adhesion bond, G, has the following relation to the work during debonding:[33a]

$$G = W[1 + \Phi(\nu,T)] \tag{4}$$

where Φ is the energy dissipation term, which is dependent on the debonding rate ν and temperature T. These calculations can be applied to AFM studies by examining the force of adhesion that the measurement provides. These can be used in the DMT model of the Hertzian mechanics:[33a,b]

$$F_{DMT} = -1{,}5\pi RW \tag{5}$$

where the F_{DMT} is the force described by the DMT model, where the attractive interactions are presumed to be outside of the contact area of the AFM tip. R is the functional radius of the tip. The energy of the surface of the material can be calculated from interactive forces on the probe tip.[33b]

$$E_s = \sqrt{\frac{P_S^3}{36\pi WR}} \tag{6}$$

In equation 7, E_s is the energy of the surface and P_S is the stiffness of the probe, also known as the spring constant. Using these values, the energy of the surface can be determined and compared, as it relates to the difference of the probe.

4 Graphene transfer with PMMA

4.1 Properties of PMMA

PMMA belongs to the acrylate family of polymers. It is an amorphous polymer with a melting point of 180 ℃, glass transition temperature between 93-126 ℃ and 20-25 ℃ in acetone (C_3H_6O).[9] The structure of PMMA is given in figure 5. PMMA creates a strong polymer due to hydrogen bonding. The monomer of PMMA is methyl methacrylate (MMA), which is synthesized by different methods.[9,37,38] Using the pure monomer to produce PMMA makes the polymer less contaminated. This way the final product is not affected by moisture or other contaminants, which contribute towards an inferior product considering its properties.[37] One of the precursors for the synthesis of MMA monomer is $[(C_5Me_5)_2SmH]_2$ which can be used at temperatures as low as 0 ℃.[38] The most common method for the polymerization of MMA is by melting, in which the precursors are heated under controlled pressure.[9,37] Many factors may affect the qualities of PMMA, such as the temperature under which the polymer forms and the materials used. For example, the use of plasticizer with MMA can greatly affect the thermal properties of the formed polymer. Some examples of plasticizers are bis(2-ethylhexyl) phthalate (DEHP) and diisononyl phthalate (DINP). The use of plasticizers can also affect other physicochemical properties of the PMMA polymer. A high concentration of plasticizer may lead to more frequent scissions between the chains, an increased surface hardness, temperature thermal degradation, bubble-like defects, and a higher UV fluorescence.[37] PMMA polymer is a popular material used in many industrial applications due to its facile synthesis and reusability. PMMA is environmentally friendly compared to other materials as it can be recycled multiple times.[39] Wan *et al.*[39] managed to recycle PMMA for four consecutive cycles at laboratory conditions. This was achieved by washing PMMA samples with bleach, which was then removed by ethanol. The PMMA samples were then put into a hydraulic press system at 210 ℃ and pressed by 44.5 kN of force for 15 minutes. This created an 800 μm of PMMA layer. The devices were used for biological experiments while the process was repeated. They concluded that their proposed process did not contaminate the biological samples and created a stable and reusable PMMA material. They also noted that the process could be improved by adding an additional cleaning step to remove major debris from the recycled PMMA.

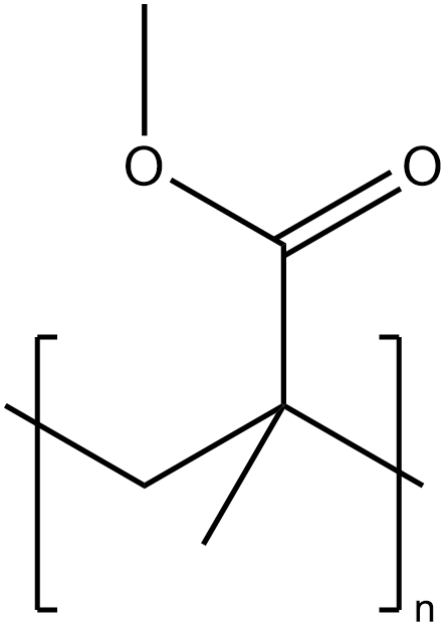

Figure 5: Th chemical structure of PMMA.[9,37,38]

4.2 The general use of PMMA

PMMA polymer has several applications in industry. It is used in furniture construction, such as tables, cabinets, and table mats, as it improves the materials' toughness and can be applied in any desired color on the surface of the furniture. PMMA is used in windows, door profiles, and panels, due to its transparency and good heat isolation properties. These properties also allow PMMA to be used in more challenging applications like greenhouses and aquariums.[40]

PMMA is also used in technological applications, like LED-lights, as it increases the light emitting potential, for LCD/LED television screens and other electronic equipment displays as it toughens the screen. Thanks to its UV-resisting properties, PMMA is also used in solar panel covers. Finally, PMMA finds use in the medical field as a fabrication material for medical tools. In addition, due to its bio-compatibility, it has been used for injectable materials, such as bone cement and cavity fillings.[40]

4.3 The use of PMMA with graphene

PMMA is used for transferring graphene, as it is an amorphous polar polymer. This means it is dissolved in solvents that don't affect graphene chemically, for example, acetone, an excellent solvent for PMMA removal. PMMA provides a good support layer on top of graphene during the transfer process which enables its protection. For a successful transfer, the target substrate must interact with graphene more strongly than the support layer. PMMA achieves this, as the polymer is easily removed and withstands the etching procedure.[7]

PMMA and graphene are also used for the fabrication of PMMA/rGO composites. These can be created by synthesis or sheet casting. The composites are made from a mixture of synthesized rGO and the MMA monomer in a solvent. Depending on the application, different methods are used. The composites have better thermal stability at temperatures below 300 ℃ than rGO itself. However, they show a great drop in thermal stability between 300 and 400 ℃. This makes them less stable at higher temperatures than rGO. However, in all cases, the composites show better thermal stability than PMMA. The sudden drop in thermal stability is due to the degeneration of weaker interactions, like van der Waals forces, between the molecular chains. This occurs when the excess PMMA breaks down. The mechanical properties of the composites exceed those of PMMA by a good margin. An increased concentration of rGO makes the composites less elastic and more fragile. Such composites find use in gas barrier coatings, strain sensors, antistatic formulations, and EMI-shielding/microwave-absorbing materials.[16]

4.4 Challenges in PMMA use for the graphene transfer process

The most common problem in PMMA use for the transfer process is the presence of residues on top of graphene after removing the PMMA layer. These residues can affect the conductivity and other properties of graphene. The main problem is the lack of solvents that can dilute PMMA completely, leading to a small layer of residual PMMA on top of the surface. When PMMA chains are cleaved during the cleaning process, the forming residual carbon chains have multiple saturated and unsaturated sections. These sections can interact with graphene via $\pi - \pi$ interactions. This relatively strong interaction makes the residues difficult to remove.[7] Several different techniques have been tested

to create ultra-clean graphene. Common approaches include the annealing of graphene under oxidizing or reducing atmosphere. Annealing occurs between 300-500 ℃. This temperature leads to the spontaneous oxidation of graphene.[17] Graphene is usually treated under a hydrogen atmosphere to reduce its surface and potential residues. To proceed with oxidation, carbon dioxide is used for an efficient level of oxidation. Other gases like oxygen (O_2) and nitrogen trioxide (NO_3), oxidize the sample strongly leading in damaging graphene. Other studied methods to remove PMMA residues include plasma treatments, ion beam treatments, mechanical cleaning, and electric cleaning.

4.5 PMMA removal methods

The challenges in PMMA transfer are well known and documented in scientific literature, while several research groups have proposed alternative methods to remove the PMMA layer and other contamination from graphene.[7]

4.5.1 Atmospheric cleaning

PMMA can be removed from the surface of graphene by exposing it to a different atmosphere. A vacuum atmosphere removes efficiently the polymer, while it does not affect graphene greatly. In addition, heating graphene allows the polymer to be removed which in the absence of oxidizing or reducing gasses, it is not reduced or oxidized. The vacuum annealing also increases the strength of interactions between the final substrate and graphene. The success of this process depends on the strength of the applied vacuum.[7]

Annealing under an inert atmosphere can be used also to remove the PMMA polymer. The atmosphere consists of a gas that is stable at high temperatures, like nitrogen (N_2) or a noble gas like argon (Ar). Under an inert atmosphere, the PMMA residue is dehydrogenated, forming polymeric chains that consist of sp^2 and sp^3 hybridized carbon atoms. This method has some limitations though, as the inert atmosphere does not have strong enough interaction with the residual carbon for it to be detached from the surface. However, an inert atmosphere can be used to remove larger contaminates, but it falls short in the case of smaller contaminants.[7]

A reductive atmosphere consists of a reductive gas, such as hydrogen (H_2) that is combined with an inert gas, like argon. The annealing removes the carbonyl functional groups. This process is effective at temperatures above the melting point of the PMMA polymer. As the PMMA residues break, they interact with hydrogen rather than graphene, preventing further contamination. This results in cleaner and slightly reduced graphene.[7]

An oxidative atmosphere is promising for effective annealing. Oxidation breaks the carbon bonds with the least energy. By oxidization, the residues of PMMA react with the oxidative environment and can be removed from the surface of graphene. The problem with this method is the oxidization strengths of different compounds. For example, carbon dioxide (CO_2) can be cleaved and release oxygen atoms while still can be reactive under the applied atmosphere.[7]

$$CO_2 + C \longrightarrow 2\,CO \tag{R2}$$

The oxidation strength is an important factor for annealing, as too intense oxidation conditions could oxidize also graphene causing tears and holes. Therefore, oxidative strength, time, and temperature are key factors to consider for this process.[7]

4.5.2 Light treatment

Visible light treatment can be used to remove PMMA from the surface of graphene by heating its surface at a temperature over which PMMA breaks. UV light can be used to weaken the interactions between PMMA and graphene. Light with a wavelength between 250 and 300 nm interacts with the carbonyl groups of PMMA. This leads to the removal of the PMMA polymer without the risk of forming new bonds. A light treatment does not introduce new elements during the cleaning, meaning no contaminants are formed further on top of graphene.[7]

4.5.3 Plasma treatment

An alternative approach to clean graphene of the residual PMMA is the use of plasma. Here, plasma composed of unionized particles, ions, and electrons, is applied on top of

the sample. The high-energy particles induce chemical reactions at functional groups and cause grafting, oxidation, reduction, or cross-linking. This technique is inspired by the patterning procedures applied in the semiconductor industry, where nano-scale circuits are constructed using plasma etching. Graphene can be treated with oxidizing, like oxygen, and reductive plasma, like hydrogen, to obtain cleaner graphene and to prevent damaging its surface. The downside of plasma treatment is the potential damage of the substrate beneath the graphene which may cause contaminants to attach to graphene. In contrast to atmospheric cleaning, plasma treatment, employs reductive gasses that produce better results than oxidative gasses, as oxidative gasses tend to cause damage to graphene. Inert gasses can be relatively harmful to graphene, as they can initiate the etching of materials from the process chamber which may end up on top of graphene. The mixture of inert and reductive gasses allows good control of the etching rate, and the process can be performed under a milder environment than a pure inert gas. In plasma treatment, although there is a potential for effective cleaning, the high-energy particles cause contamination and damage to graphene.[7]

4.5.4 Ion beam treatment

The use of high-energy particles to remove PMMA residues is a useful technique for plasma treatment. However, it affects the surrounding area and adds contaminants rather than cleaning the surface. This leads to the possibility of studying the removal of PMMA residues using high-energy particles in a beam. An ion beam provides a focused area that cleans only the contaminated part of graphene rather than the whole graphene surface and the substrate on which it sits. The use of inert gas is thus favored, as the intensity of the beam can be controlled, and it does not damage the surrounding area. Noble gasses like helium and argon are good candidates to remove PMMA residues, due to the high energy they can deliver on the surface. Another approach towards cleaning is the use of an electron beam. The electron beam excites the contaminated particles by introducing an excess number of electrons to the particles. The large increase in electron concentration and energy causes the molecules to break down. With this treatment, there are no additional elements introduced to the treatment. The challenge, however, is that the high-energy electron beam can cause serious damage to graphene beneath the treated area if the intensity of the beam is not efficiently controlled.[7]

4.5.5 Mechanical cleaning

Mechanical cleaning is a method that uses physical interactions to remove contamination. The most important aspect of mechanical cleaning is that it does not affect graphene chemically, as no reactive compounds are present during the cleaning process. Mechanical cleaning can be performed by AFM. Using the contact mode in AFM, the surface of graphene is swept by the tip. This way, the interactions between contamination and graphene are broken while any contamination is swept away. The challenge is to find the correct contact energy for the cleaning process so that graphene will not be damaged. AFM cleaning is referred to as a micro-cleaning operation, due to the small processing area which can be performed over one cycle. Macro cleaning operations process larger areas over one cycle but with lower accuracy. The larger area process allows us to approach potential purification issues in different ways, for example, consider the conductive properties of graphene and use therefore electrostatic forces to remove any residual PMMA. The electrostatic-force cleaning can be applied using a positively charged rubbing cloth that sweeps close to the graphene surface without touching it. The electrostatic pressure between the cloth and graphene creates a high temperature that melts PMMA residues and removes them. Another approach to macro-cleaning is to use an active carbon-coated roller. The roller is rolled repeatedly on top of graphene, removing the amorphous and residual carbon contamination due to the higher interaction with the active carbon. The advantage of these cleaning methods lies in their simplicity and ability to clean a large area efficiently.[7]

4.5.6 Electric cleaning

Based on the conducting properties of graphene, electricity can be used to clean its surface from less conductive carbon-based contamination. One way to remove PMMA is electrolysis. In this process, the post-annealing graphene is installed into an electrochemical cell. An acid is used as the electrolyte and the process forms hydrogen, which interacts with the PMMA residues and removes them from the surface. Alternatively, the use of current electricity may be applied for graphene's purification. When current is run through graphene it heats up, resulting in the removal of PMMA and other contamination. The method is similar to annealing, however, only graphene is heated and not the area or the atmosphere around it.[7]

5 Graphene transfer using gels

During the transfer process of graphene a polymer is used as the support layer.[4] Polymers are stable materials, that are relatively stiff and hard to remove completely. This leads to the study of alternative materials for the transfer process. In the following sections, the different properties of transfer support gels (TSGs) are investigated. Using graphene in conjunction with a certain type of gel can lead either to desired or undesired interactions.

5.1 Gel basics

At the molecular scale, in biological systems, the self-assembly event of biomacromolecules is a dynamic process immediately related to structural, metabolic, signaling, and homeostatic functions. For example, proteins, nucleic acids, and sugars fold toward certain configurations and form assemblies to achieve their functional role. The self-assembly event occurs when the active sites on the molecules form inter/intramolecular supramolecular bonds. At first, the concept of self-assembly seems complicated, for example in the case of proteins, however, the formation of higher-order architectures may be studied at different organizational levels such as the primary, secondary, and tertiary organization events. The long polypeptide chains provide active sites, distributed spatially by chain folding, leading to assembly events of different organizational levels. In the case of artificial soft materials (gels), the self-assembly process is achieved by the self-organization of smaller molecules (gelators) under certain conditions.[41]

Gels consist of a supramolecular network of molecules(matrix) formed by the self-assembly of the gelator molecules. Gels can be divided by the bonding method into chemical and physical gels. Chemical gels are held together by chemical bonds, such as covalent or ionic bonds. Chemical gels don't occur naturally as their formation requires a lot of energy and specific treatments. Therefore, chemical gels can only be artificial materials with networks at the macromolecular scale.[41] Physical gels are more common, as they form with non-covalent intermolecular forces, like hydrogen bonds and Van der Waals interactions. Supramolecular gels are always physical gels.[41,42]

Gelation can be induced either by external stimuli or occur spontaneously. For example, gelation may be triggered by exerting energy on the system by heating, changing the pH

of the system, or exposing it to radiation. These techniques require a gelator, that has an active unit (functional group) that responds to specific stimuli. Each of these techniques affects the supramolecular composition of the gel matrix leading to materials with different physicochemical properties while they may trigger gel-to-sol or sol-to-gel transitions.[41,42,43] Van der Waals interactions, hydrogen bonding, hydrophilicity, hydrophobicity, aromatic-aromatic, and electrostatic interactions are examples of non-covalent intermolecular interactions which lead to the self-assembly of the gelators and the formation of aggregates, which encapsulate solvent molecules forming gels.[42]

Gels are also classified according to the used solvent. In the case of water, the gelators are called hydrogelators, and the corresponding materials are hydrogels.[41,44] These supramolecular gel systems form by van der Waals interactions, hydrogen bonds, or weak stacking of the π-π orbitals. The most characteristic properties of hydrogels are their ability of swelling and the permeability of their matrix. The structure of the hydrogel can be manipulated by introducing or removing water from the gel. The hydrogel can swell to a larger size and be less viscous. Hydrogels can also be dried and form films. Hydrogels have been explored in medicinal and biological applications due to their biocompatibility.[44]

When organic solvents are used, the gelators are known as organogelators, and the corresponding materials organogels.[41,44] The formation of organogels is similar to that of hydrogels, as the same interacting forces apply. However, in organogels, the properties of the solvent, for example, polarity, affect the self-assembly and the forming gel. The effect of gelators and solvents on the self-assembly process is constantly studied. When designing new organogelators/organogels, certain structural requirements need to be met for the formation of gels.[44]

Supramolecular gels are classified as physical gels, as they are held together by physical interactions. Supramolecular gels come in many different sizes, structures, and qualities, making them a huge area of research. Supramolecular gels can possess a reversible gel-to-sol phase transition that can be manipulated by heat, chemical, or radiation stimuli. This allows them to be applied to sensor technologies, oil recovery from water mixtures, medians for crystal growth, and control release of pharmaceutical molecules. There are multiple types of supramolecular gels, such as metallo-gels, which contain a metal ion as a ligand in the structure, and liquid crystalline physical gels, which are microphase-separate composite structures that form gels.[43]

In this thesis, both polymeric and physical hydrogels have been used.

5.2 Gel thermodynamics

To understand the developed intermolecular forces in physical gels, it is beneficial to study the contributing factors of gel formation. For polymer gelators, this can be done by examining the total free energy density function (Z) of the system. The total free energy of the system (Z_{tot}) can be obtained by integrating the energies over the volume (V) of the gel.[45]

$$Z_{tot} = \int_V Z dV \tag{7}$$

It is also possible to understand Z by breaking it down to its components. The energy density consists of the cross-link bond energy (Z_{bond}), the elastic energy of the gelator ($Z_{elastic}$), and the mixing energy of the gelator and solvent (Z_{mix}). Each of these elements contributes to the total energy density function.[45]

$$Z = Z_{bond} + Z_{elastic} + Z_{mix} \tag{8}$$

When studying the Z_{bond}, it must be assumed that the cross-linking bonds have the same structure. In this way each bond can contribute equally to the bonding energy. The energy then consists of the energy required to break the cross link bond (E_a) and the cross-link density (q).[45]

$$Z_{bond} = -qE_a \tag{9}$$

The variable q is an important part of the energy density calculation, as it brings the density dimension into the calculation of bond energy. E_a gets its value from the characteristic time for reconstruction (τ), the temperature (T), the Boltzman constant (k) and the time dimension prefactor A.[45]

$$E_a = kTln(\frac{\tau}{A}) \tag{10}$$

As it is important to understand the cross-link bonding in the gel, it is also important to understand what happens outside of the cross-links. This is more challenging, as the length of sections between cross-links can vary in size. The density element in this function is related to the random lengths of The non cross-linked molecular chains in a cubic lattice (s) and the number of gelator molecules allocated at each cross-link section (evolution of gelator density (ϕ)). The change of free energy (ΔE_F) must also be considered while calculating the $Z_{elastic}$.[45]

$$Z_{elastic} = \frac{\Delta E_F}{s/\phi} \tag{11}$$

The change of free energy (ΔE_F) derivers from the temperature dependent change of entropy (ΔS) in the gels structure.[45]

$$\Delta F = -T\Delta S = \frac{3}{2}kT[ln(2\pi s) + \frac{M_{kk}}{sb^2} - ln(3)] \tag{12}$$

In the equation, M_{kk} is the connectivity tensor and b is the Kuhn length of the gelator. The final parameter in the energy density of the system represents the mixing energy density (Z_{mix}). This is obtained quite simply, by studying the volume fracture of the gelator (V_c) and its hydrophilicity by the use of Florfy's dimensionless parameter (χ).[45]

$$Z_{mix} = kT[\frac{\mathrm{v}_c}{s}ln(\mathrm{v}_c) + (1 - \mathrm{v}_c) + \chi \mathrm{v}_c(1 - \mathrm{v}_c)] \tag{13}$$

The free energy density function allows us to study different aspects of the gel formation and its qualities mathematically. These calculations may be helpful in deciding the type of used solvent or the gelator concentration to achieve and help to predict also the characteristic properties of the formed gels.[45]

5.3 Graphene in gels

Combining graphene with gels is not a new approach in the field of graphene-based materials. There are different ways to combine graphene with gels to achieve sophisticated materials with desired properties. Wang *et al.*[10] has synthesized a magnetic 3D nitrogen-

doped graphene gel by the hydrothermal self-assembly of GO. The gel showed excellent superparamagnetic properties. It could be manipulated with a magnet, without any direct contact, while isolated in a glass jar. Regarding the structure of the gel, graphene provides the structural backbone to the system that is light and can be easily manipulated by the magnetic forces which affect the iron (Fe) compounds within the gel network. This gel could replace precious metal catalysts like palladium (Pd) or gold (Au). This is important since the industry requires cheaper and easy-to-prepare catalysts for chemical reactions towards greener chemical processes.[10]

Graphene-based gels have also been used in sensors. Zhang *et al.*[3] reported the recent development of 3D graphene-based gels and their applications. These organic gels have many properties which make them excellent materials for multiple uses. Such properties include high absorption levels, specific surface area, stability, enhanced active sites, and a photocarrier meditator ability. These properties allow gels to be used in many applications, such as removing organic, gaseous, and heavy metal pollutants, and for bacterial treatment applications. The gels have found use also in photocatalytic actions while multiple studies on this subject have been published.[3] Especially the photo-thermal effects of these gels are promising for several applications. Near-infrared light improves the photocatalytic effect of a graphene gel film. This treatment could be used in pollutant purification. Additionally, gels in conjunction with graphene-based composites are promising materials in purification processes.[3]

5.4 Using gels as a support layer

An alternative approach for obtaining ultra-clean graphene is to use a gel as a support layer. Gels may be considered a good option for graphene transfer because they are rigid enough to maintain a stable shape during the transfer process while they can act as a shock absorbent, which prevents the formation of wrinkles on graphene during the transfer process.[6] To achieve graphene transfer by gels, they should be easily applied on top of graphene, attach effectively, and be easily removed after the transfer. One option for these gels is to use n-doping adhesive gel buffers. Such material was introduced in the article "Defect-Free Mechanical Graphene Transfer Using n-Doping Adhesive Gel Buffer" by Seo *et al.*[6] In the article, the authors produced an n-doping adhesive gel by mixing branched polyethylenimine (PEI) and glutaraldehyde (GA). Polyethylenimine was used, as a strong

n-type charge transfer dopant of graphene, and glutaraldehyde as a cross-linking agent. The PEI-GA composite gel was then applied to graphene by spin coating. On top of the spin-coated gel, a support substrate was added to keep the product clean. The support layer was then added on top of the graphene/Cu layer via roll press. The sample was then heated at 160 ℃ and quenched by hydrogen flow which converted the mixture to a soft crosslinked gel. Graphene was removed from Cu by direct mechanical delamination and moved to the target substrate. When the Raman spectrum was measured from the transferred graphene, there was a clear red shift on the G-band and a blue shift of the 2D-band. This is caused by the n-doping of graphene after the application of the PEI-GA layer. The group investigated the adhesion energy between the surfaces and found out that the adhesion energy between graphene and PEI-GA is larger than between graphene and copper. The group concluded that defect and etchant-free graphene could be created using a gel layer. The soft viscoelastic PEI-GA gel enables the mechanical delamination of graphene due to the gel's stress relaxation characteristics and the charge-transfer interaction with graphene. This allows the direct delamination transfer to be performed without any mechanical defects.[6]

For a gel to be used as a support layer for graphene transfer, it should be easily removed from the surface without damaging graphene. Gels can be tuned by external factors, like temperature, pressure, acidity, and radiation. These factors can affect the structure or the mechanical properties of the material during its formation or deformation. The gel network can be affected by ultrasonic treatment and the speed of cooling. Ultrasonic treatment helps to create more elastic gel networks. This is most likely due to the small structural parts that attach to each other with significant interaction force. A rapid cooling speed increases the storage modulus but creates fragile structures in the gel network. In hydrogels, the rapid cooling causes the formation of smaller fibers. The smaller size of fibers allows more water to be encapsulated, thus making the freezing of the gel faster, however, the material is less dense and stable.[46]

5.5 Acid resistant gels

The removal of copper or any other catalytic metal surface during the graphene transfer process is usually done by an acid bath, where the catalytic metal layer gets removed.[4,5] This is why the TSG should be resistant to acidic or oxidizing agents. One option would be

to use acid-resistant preformed particle gels (AR-PPG), which have a good deformation ability and stability under acidic conditions.[47] Zhou *et al.*[47] studied the formation and properties of acid-resistant preformed particle gels (AR-PPG Figure 6). The physical and chemical properties of the formed gel were also studied by placing the material in an acidic solution (pH 3) and heating it. The swelling and structural transformations were studied by a laser particle size analyzer. The heating was studied by thermogravimetric analysis (heating from 40 to 800 ℃ at increments of 20 ℃ per minute).

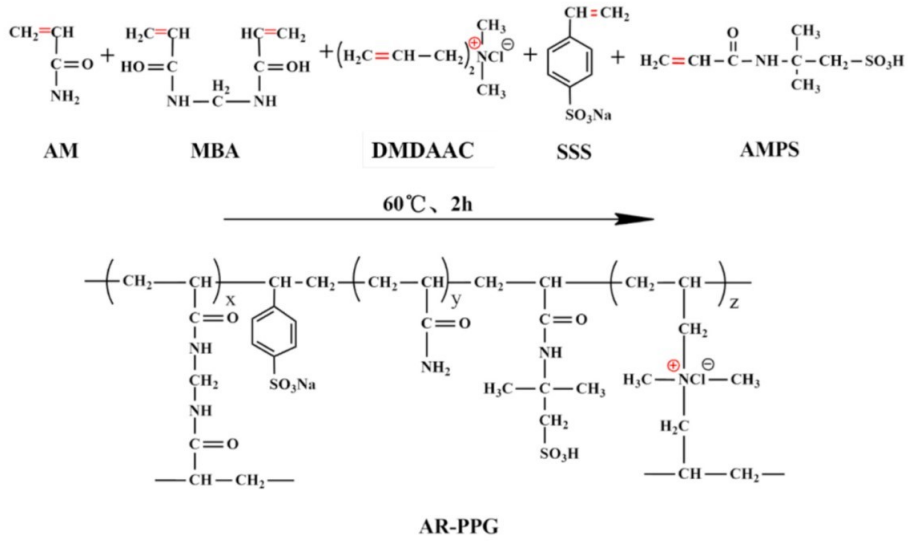

Figure 6: Synthesis of AR-PPG. Adapted with permission from Zhou, B., Kang, W., Yang, H., Zhu, T., Zhang, H., Li, X., Sarsenbekuly, B. and Sarsenbek, T., Preparation and properties of an acid-resistant preformed particle gel for conformance control, Journal of Petroleum Science and Engineering, 2021, 197, 107964.[47]

Swelling studies revealed that the structure of AR-PPG remained stable under acidic conditions. Intermolecular hydrogen bonds are formed between the amide groups of the chains which reduce the swelling of the gel. This leads to electrostatic repulsion between the cationic groups and protons of the acid. In addition, sulfonate groups are not affected by external acidity or alkalinity, because of their strong polarity. Such factors prevent the gel from shrinking in an acidic environment or breaking in an oxidative environment. During thermal tests, AR-PPG showed three distinct faces. Between 40 and 220 ℃, the gel structure was changing, due to the vaporizing of moisture and the cleavage of the oligomers. From 220 to 400 ℃ the amide, carboxylic and sulfonic groups started to cleave. Above 400 ℃ the polymer chains and intermolecular bonds begin to break down causing

the gel to lose mass. This experiment revealed good thermal stability of the chains and the gel components.[47]

5.6 Heat applied transfer

Depending on the gelator molecules, gels can react in different ways to temperature changes. The formation of strong hydrogen bonds can be promoted by increasing or decreasing the temperature, accordingly. Heating/cooling allows gelation to occur, usually during the cooling process, where the gelator molecules spontaneously self-assemble to form a gel after external heat is applied to the system. Additionally, the mixing of different types of gelator molecules can increase or decrease the thermal stability of the gel, respectively. The most crucial factor in gel stability is the development and type of supramolecular interactions. Hydrogen bonds are more stable and heat resistant than carbamate–carbamate interactions.[42] Chevigny *et al.*[11] created an organogel, which is stable at room/ambient temperature but collapses at 55 ℃.[11]

As the properties of gels depend on the type of gelator molecules, their thermal stability can be tuned to produce gels with desired thermal properties. Moffat *et al* .[42] studied the effect of three chemically different organogelators. These had peripheral carbamate groups protected by the Boc group, which formed fibers of 80 nm in diameter, amide linkages connected by long alkyl chains, which formed fibers of 20 nm in diameter, and a meta-substituted aromatic ring based on peripheral amide groups that produced fibers between 10-20 nm in diameter. The gel structures are given in Figure 7. Gels prepared at different gel concentrations were heated, and the melting point was recorded. From the experiment, it was clear that the alkyl chains were effective thermal stabilizers. Indeed, the alkyl chains showed a thermal stability over 80 ℃ above a concentration of 25 mM. The carbamate group showed 31% of the alkyl chains thermal stability and the aromatic ring was around 75%. When gelators bearing the alkyl chains were mixed with those bearing the less stable carbamate group gelator, the thermal stability of the mixture increased to that of the alkyl chain derivatives. This suggests that the carbamate gelator had no effect on the thermal stability of the gel in the mixture. On the contrary, by mixing alkyl chains and aromatic rings, the gels' thermal stability was reduced, by approximately 44% compared to the alkyl chain derivatives. This study demonstrates the importance of chemical bonding in gelation and its effects on the thermal stability of the formed gel.

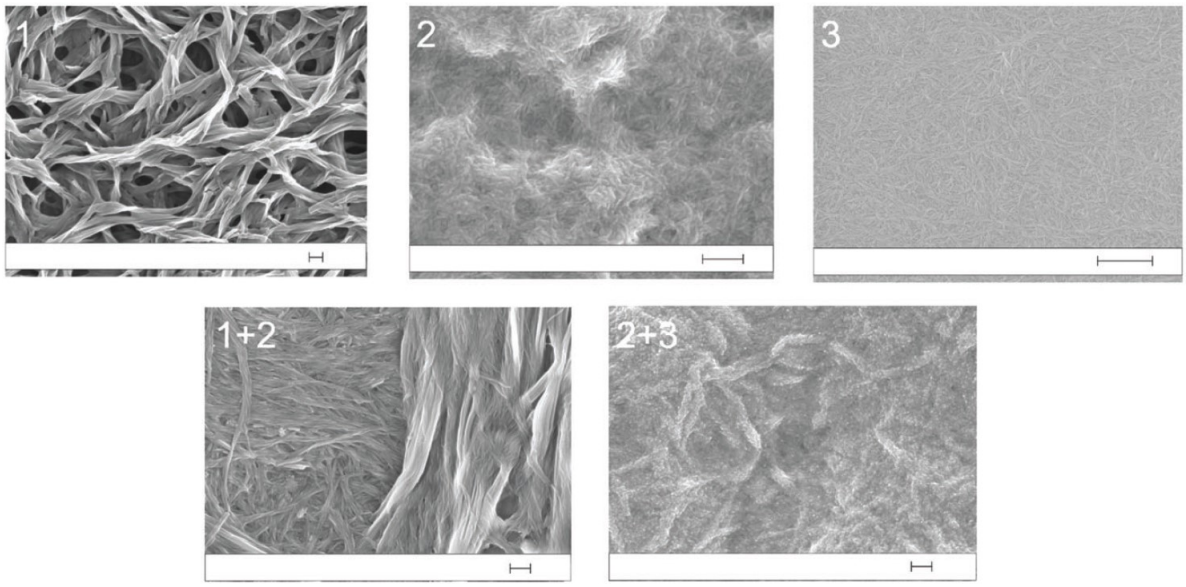

Figure 7: Images of dried gels from styrene–DVB of alkyl chains (1, upper left), carbamate group (2, upper middle), aromatic ring (3, upper right), a self-sorting equimolar mixture of 1 and 2 (lower left), a non-sorting equimolar mixture of 2 and 3 (lower right). Images have been taken with a field emission gun scanning electron microscope. Adapted with permission from Moffat, J. R. and Smith, D. K., Controlled self-sorting in the assembly of 'multi-gelator' gels, Chemical Communications, 2009, 316–318, Copyright 2002 American Chemical Society.[42]

5.7 Biocompatibility

Many gels interact with biological systems. Some gels possess antibacterial properties and are used to treat simple infections or other deceases. Antibacterial gels are, easy to apply and remove.[12] Gels can also serve a secondary purpose in medical applications. For example, after application, some gels decompose as the cells use them for their nutrition. This guarantees a safe method to remove the gel that is also beneficial, for example in wound healing processes.[12,13] Antibacterial gels pose a large area of research due to the growing antibiotic resistance of bacteria.[12]

Gels have been studied also as biomaterials that mimic the properties of the extracellular matrix (ECM). These gels can be used as bio substrates for cell culture applications allowing cells to attach to the material's matrix and proliferate within an environment, which mimics ECM. This could be achieved by immobilizing proteins or peptides in the gel. The immobilization of proteins and peptides may protect them from enzymatic degradation while they affect the structural and functional properties of the gels. With bio-

conjugation, the functionalization of bio-molecules can be controlled, while the produced gel materials have those desired properties to allow implantation into a biological system. The immobilization also allows the gels to be sterilized without risking the degeneration of proteins. The applications of such biomaterials do not confine only to protein immobilization. Hydrophobic-hydrophilic gel structures, functionalized with proteins, create sophisticated surfaces for cell seeding. Surfaces as such, are responsive to environmental changes, such as temperature, and can release proteins or cells.[48]

In addition, gel can affect the cell structure (phenotype). The stiffness of the gel is a key factor in gel application and behavior of cell cultures. Different types of cells prefer a certain stiffness of gel as it benefits their proliferation and function. The gels' inner architecture is also important for the promotion of cell growth. Indeed, different gels promote cell growth differently. For example, pore-like structures promote excellent cell growth and support homeostasis.[48]

Since graphene can be used in several biological applications, the transfer gel could remain on top of the graphene monolayer for the construction of a bionic device.

5.8 Oxidizing and reducing gels

The gel structure can be affected under oxidizing and reducing environments. This makes the handling and removal of gels possible, for example, by manipulating atmospheric conditions.[47] Multiple gels have also a significantly lower gel-to-sol phase transition temperature compared to the decomposition temperature of graphene.[11,17,42,47] The combination of an oxidizing or reducing atmosphere with heat could remove the gel layer from the top of the graphene monolayer. These properties are used already for the PMMA removal methods.[7] This means that there is an opportunity to establish an optimized protocol by which the transfer support gel layer could be removed by modification of an existing method.

5.9 Optional gels for transfer

5.9.1 Hyaluronic acid gel

Hyaluronic acid (HA) was discovered in 1918, but was characterized and named in 1934.[49] HA is found in the human body at ECM. Large concentrations of HA are found in the human eye, joints, and ovum. HA is also used as a nutrient supporting cell growth in the body. This makes it an essential ingredient for wound healing processes.[13] HA interacts with cell-specific markers, for example, hyaluronate-mediate motility receptors and endocytosis receptors in liver cells.[13,49,50] After its discovery, HA has been used in clinical applications, such as aesthetic medicine, eye surgeries, and joint treatments. For many years, HA was obtained by extraction from biological materials of animal origins. Due to growing demand, the HA biosynthesis using bacteria was developed to increase production.[49] Currently, HA has multiple medical applications due to its functionality and degenerability.[13,49] One of the current research areas focuses on targeted drug delivery.[49]

Due to its chemical structure, HA gels may be prepared in several different ways, for example, in combinations with other compounds and the use of crosslinkers (Figure 8). The biocompatibility of HA motivated researchers towards new materials. The most studied cases of HA gels refer to the use of different crosslinkers. The most common crosslinker in HA gels is adipic dihydrazide (ADH), as the formed gel has excellent biological properties. New applications have also been studied based on the properties of HA gels. For example, polyfunctional epoxides interact with the carboxyl and hydroxide groups of HA forming ether and ester bonds. Some of these crosslinkers are agarose and ethyleneglycoldiglycidyl ether. These gels have been reported as promising candidates for tissue scaffolding and drug delivery applications. Changing the crosslinker can also affect the inherent properties of HA gels. Indeed, crosslinking with glutaraldehyde under acidic conditions results in water-resistant gels. In addition, carbodimides react with the HA chain, acting as crosslinkers, since they react with adjacent carboxyl and hydroxyl groups of HA, creating inter- and intramolecular cross-linked bonds.[13]

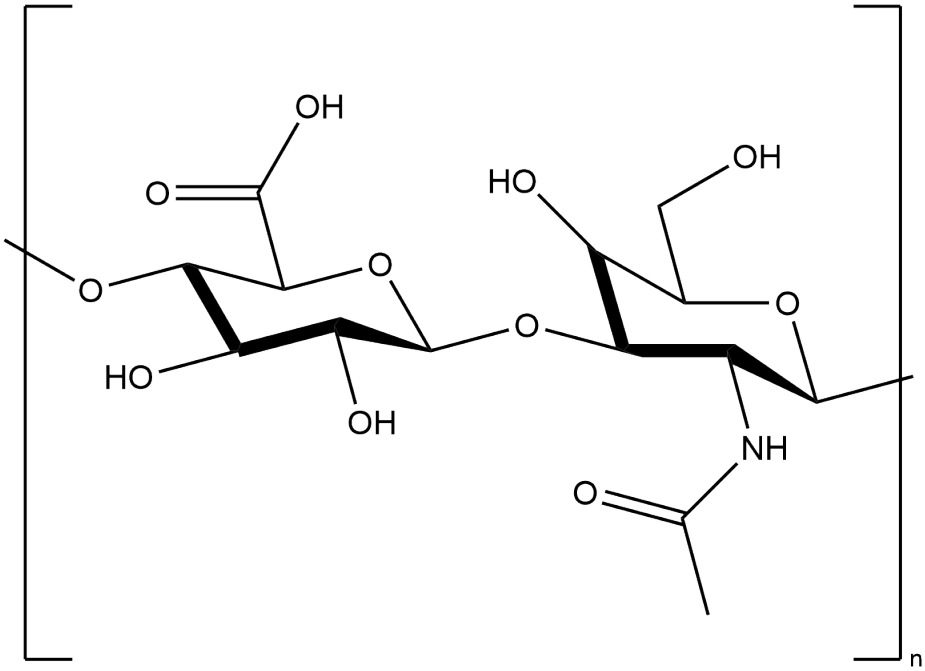

Figure 8: The chemical structure of hyaluronic acid.[50]

HA gels can also form by crosslinking divinyl sulphone with the hydroxyl groups of HA, yielding ether bonds and creating hylans (chemically crosslinked HA with divinyl sulfone).[13] Hylans have been produced as coated scaffolds by using carbon nanotube reinforcement and template leaching. They can also be combined with other HA gels to form stronger crosslinking configurations. There is also the possibility to create gels via non-crosslinking compounds, which rely completely on non-covalent interactions amongst the HA molecules. For example, HA may form a self-supporting gel by the hydrogen bonding between acetamido and carboxylate groups and hydrophobic interactions.[13] Autocrosslinked HA can be used as a nutrient boost, as its application on broken human tissue supports cell reproduction efficiently.[13] In another example, modified HA gels have been used as a growth medium for bone marrow cultures, fibroblasts, and chondrocytes. The gels were prepared by the esterification of HA or the alkylation of hyaluronan ammonium salt with alkyl halides.[13]

The Raman spectrum of HA is shown in Figure 9.[51] Two distinct features are highlighted. When the concentration of HA increases, the intensity decreases. This means that stronger bonds are formed between HA strains at lower concentrations.[51] A second notable feature is observed when the spectra are compared to the Raman spectrum of graphene (figure 3). The G-band of graphene is surrounded by peaks 5, 6, and 7 of the HA. These bands originate from the carbon-hydrogen bending, carbon-nitrogen stretching, and the amide

group.[51] This may cause interference in the Raman spectrum of the used gel to transfer graphene if the gel is not removed completely from graphene's surface. Approximately at the 2D-band position, there is no counter-effecting bands that would disturb the Raman shift.[51]

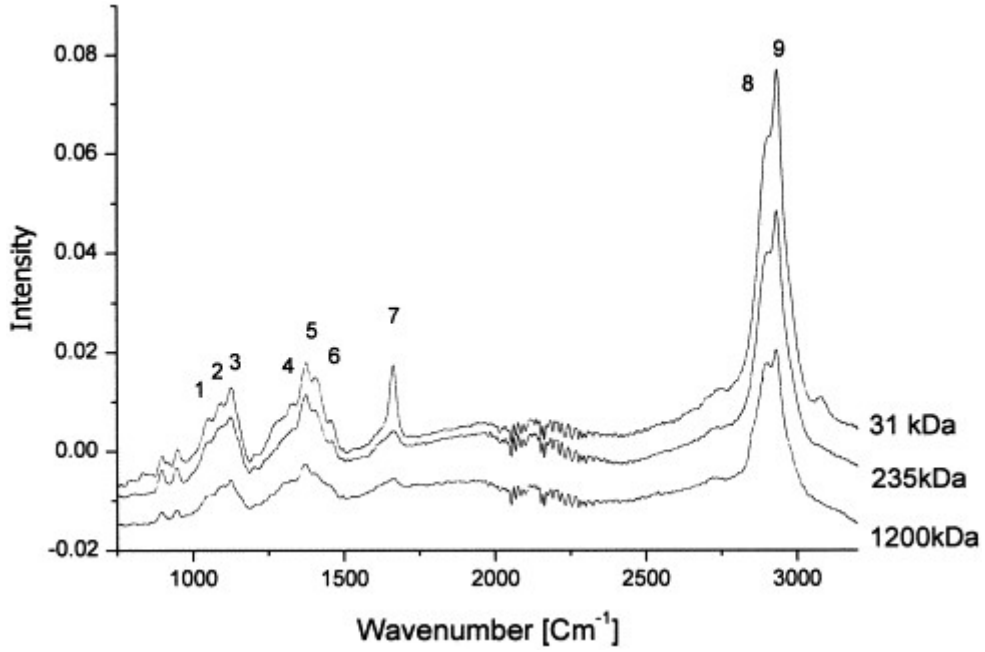

Figure 9: Raman spectra of HA in different concentrations. In the figure, Daltons (Da) is equivalent to the unified atomic mass unit (u). Adapted with permission from Alkrad, J. A., Mrestani, Y., Stroehl, D., Wartewig, S. and Neubert, R., Characterization of enzymatically digested hyaluronic acid using NMR, Raman, IR, and UV-Vis spectroscopies, Journal of Pharmaceutical and Biomedical Analysis, 2003, 31, 545–550.[51]

As HA is present in the human body, its use opens a window for the development of several materials for tissue engineering applications. The effectiveness of these materials is based on the unique properties of HA, stemming from its structure and function in the human body. HA has multiple functional groups that can interact with other molecules (Figure 8). This enables HA gels to be used as a supporting structure when introducing functional domains in ECM. Since the human body is capable of cleaving HA, it will not contaminate the extracellular matrix with toxic compounds. In addition, as it participates in the wound healing process, HA is an excellent candidate to aid in faster healing and fighting infections.[13,48] HA gels have been used as ECM-supporting structures and for the immobilization of proteins.[48]

Combining graphene and HA is not a new practice in the field of biomaterials. GO and HA can be used as drug delivery systems. GO can be conjugated with HA via ADH crosslinking. GO-HA can be used to deliver, for example, anticancer drugs directly to the tumor. With the help of the cells' hyaluronate-mediate motility receptors, the drug release can be controlled and delivered to the cell via the hyaluronic acid-receptor-mediated endocytosis.[13,50] The challenge in this treatment is the cytotoxicity of the drug delivered by the GO-HA system. GO-HA per se, has negligible cytotoxic effects to normal or cancer cells. Cytotoxicity could be controlled by the pretreatment of HA. The HA would then block multiple receptors by attaching on them, preventing the excess release of the delivered drug.[50]

HA is an excellent option for graphene transfer due to its biological application potential. The gels' ability to degenerate in the human body would open multiple different routes to attach graphene-based biosensors to the human body without the risk of toxicity Based on the aforementioned studies, HA interacts with graphene, thus experimenting with HA is a logical step for the current study.

5.9.2 Fmoc-F

The 9-fluorenylmethoxycarbonyl (Fmoc) is an aromatic group commonly used to synthesize amphiphilic gelators. Their corresponding gels can be prepared by different methods such as solvent switch, sequential pH change, or enzymatic hydrolysis of gelator precursors.[52] Fmoc-protected phenylalanine (Fmoc-F) based gels are the commonest materials derived from amphiphilic amino acids and are prepared by heating and sonication. Heating plays an important role in the Fmoc-F gel preparation, as the cooling stage activates self-assembly.[12,53]The structure of Fmoc-F is given in figure 10.[12]

Fmoc-F has antimicrobial properties and is especially effective against Gram-positive (G+) bacteria. Fmoc-F destroys the membrane of the G+ bacteria causing their death. Due to the difference in their membrane structure, the Fmoc-F does not affect Gram-negative (G−) bacteria.[54] By combining Fmoc-F gel with antibiotics the activity spectrum of Fmoc-F gels can be expanded also to G− bacteria.[12] Gaphane *et al.*[12] reported that Fmoc-F gel when combined with aztreonam (AZT) antibiotic the resulting gel is active against both G+/− bacteria without causing damage to mammalian cells. AZT was

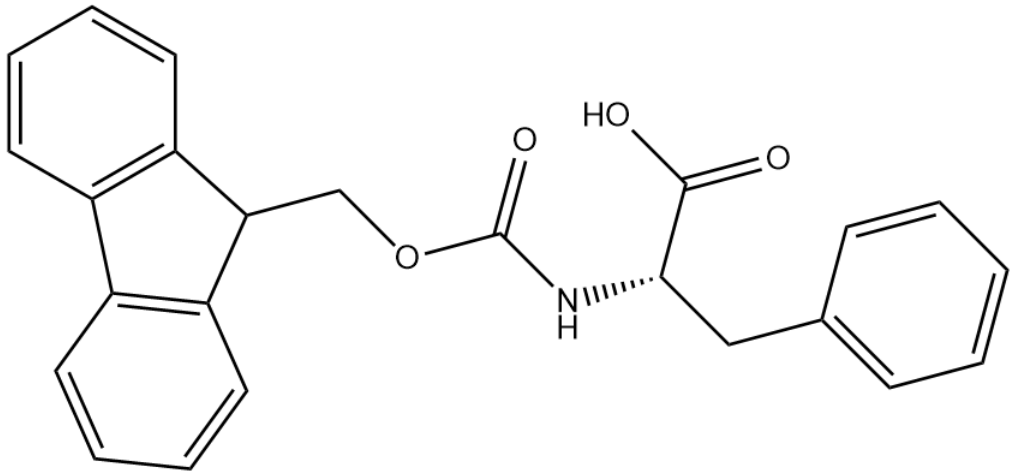

Figure 10: The molecular structure of Fmoc-F.[12]

introduced in the Fmoc-F gel during the gelation process while the material was cooling down. The gel was injected into a mouse's wound, which was previously infected with G+ bacteria (Staphylococcus aureus) and G− bacteria (Pseudomonas aeruginosa). After 48, the bacterial load decreased about a thousand-fold. The two-component gel was significantly more effective compared to individual Fmoc-F or AZT. The gel was also applied to Madin–Darby Canine Kidney epithelial cells to study its cytotoxicity. The cytotoxicity can be assessed by measuring the concentration of lactate dehydrogenase (LDH) in the cell culture. LDH is a cytosolic enzyme that is released when the cell membrane is damaged or destroyed, thus its concentration in the treated culture can be directly related to the cytotoxicity of the sample material. Cytotoxicity is expressed as the percentage of viable cells (%) compared to the untreated control sample.[12]

$$Toxicity(\%) = \frac{TreatmentLDHconcentration}{MaximumLDHconcentration} * 100 \tag{14}$$

At lower concentrations, the mixture of AZT and Fmoc-F showed negligible or no cytotoxic effect compared to the control culture. Higher concentrations resulted in an increase of cytotoxicity, up to 40%. The experiment showed that the Fmoc-F gel can be used as an antibacterial material while it is biocompatible with mammalian cells and causes no harm to the environment.[12]

The Fmoc-F antibacterial properties allow the material to be used for the removal of biofilms from infected tissue. As the infection becomes chronic, bacterial biofilms pose a challenge, because the films promote antibiotic resistance in the infection site.[55] Singh *et al.*[55] reported the efficiency of Fmoc-F films against S. aureus and P. aeruginosa bacteria. The Fmoc-F gels kill G+ bacteria, thus the removal of the S. aureus bacterial biofilm is removable by default. G− bacteria are affected by the Fmoc-F interaction with the forming ECM, rather than the bacteria itself. Fmoc-F interacts with the ECM by creating micelles that trap hydrophobic ECM components, preventing this way its formation if a biofilm has already been formed. Fmoc-F does not need to be applied for the removal of the biofilm. The group studied if the biofilms could be formed on top of a Fmoc-F gel surface. The results were straightforward. Fmoc-F gel prevents the formation of a biofilm mostly or completely. This is most likely because of the amphiphilic nature of Fmoc-F, hindering the hydrophilic conditions required for the formation of the biofilm.[54,55] This allows Fmoc-F to be used as a coating material in different, sterile required surfaces. As previously mentioned, in this case, the Fmoc-F gel could be combined with antibiotics to counter the biofilm antibiotic resistance and treat the bacterial infection more efficiently.[55]

The Raman spectrum of Fmoc-F is given in figure 11.[56] The area around the D-band is active, as expected considering the Fmoc-F's structure (Figure 10). This indicates that the contaminant gel would be detected as it would increase the band intensity if present after transfer and cleaning. The area over 1700 cm^{-1} would not be affected by the gel residue.

Fmoc-F has multiple aromatic sections in its structure that could interact with graphene in the gel. It also possesses hydrophilic groups in the middle of its structure, making it able to interact with hydrophilic solvents. Fmoc-F could be an excellent gel for the transfer of graphene monolayer, as it can interact with the graphene and be removed using protic solvents.

5.9.3 BocFFOtBu

The *N*-tertbutyloxycarbonyl (Boc)–L-phenylalanyl–L-phenylalanine tertbutyl ester (BocF-FOtBu) was studied by its properties reported in the article by Chevingy *et al.*[11] The Boc and tert-butyl ester groups are commonly used as protective groups in organic synthesis.

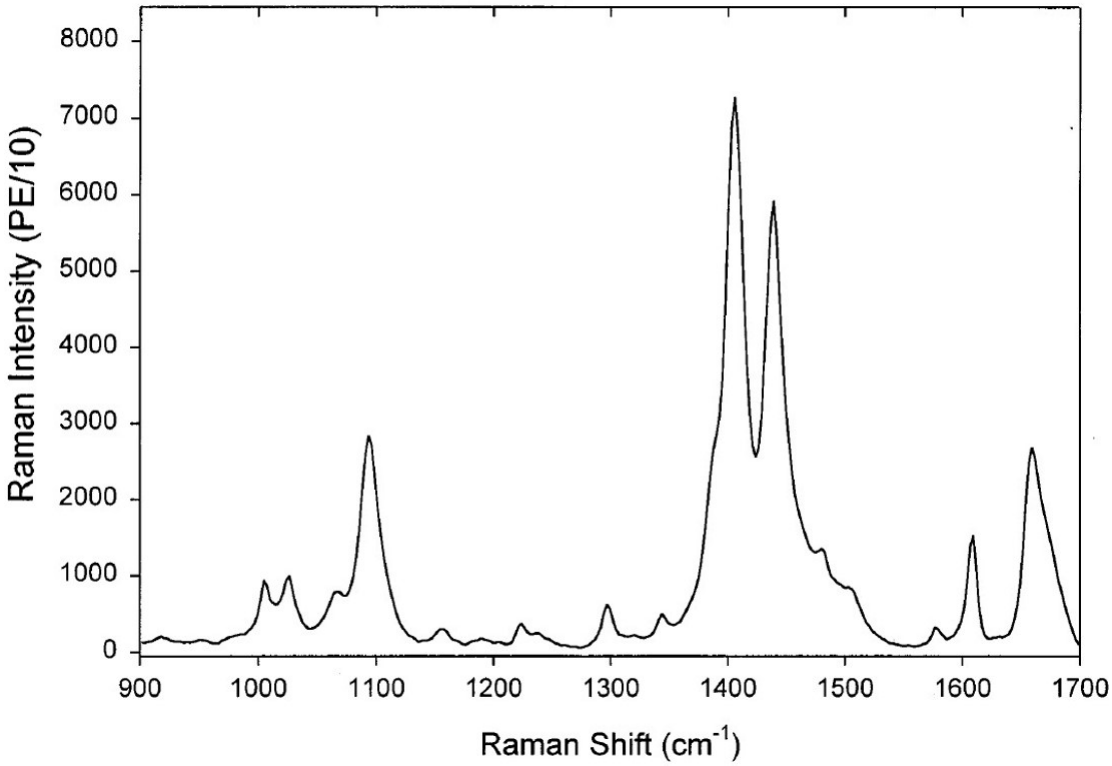

Figure 11: Time-dependent Raman spectrum of Fmoc-F. Adapted with permission from Houlne, M. P., Sjostrom, C. M., Uibel, R. H., Kleimeyer, J. A. and Harris, J. M., Confocal Raman microscopy for monitoring chemical reactions on single optically trapped, solid-phase support particles, Analytical Chemistry, 2002, 74, 4311–4319. Copyright 2002 American Chemical Society.[56]

The deprotection of the Boc group in the presence of the ester group is irreversible, thus making the forming product stable in ambient conditions.[57] The gel can be created from the BocFFOtBu precursor gelator by suspending it in tert-butyl acetate (tBuOAc) solvent and adding sulfuric acid to initiate the Boc deprotection, which triggers the gelation process. The selective deprotection process and gel formation are shown in figure 12.[11,57] The forming gel is stable for four days, after which it breaks down into a solution. However, its lifetime can be extended by swelling the gel in (tBuOAc) solvent. The swelled gel is found stable after seven months. Another interesting property of this transient gel is its transition temperature (gel-to-sol). The gel is stable up to 50 ℃ and breaks down at 55 ℃. The gel reforms after cooling down. This means that the gel-to-sol process is thermoreversible.[11]

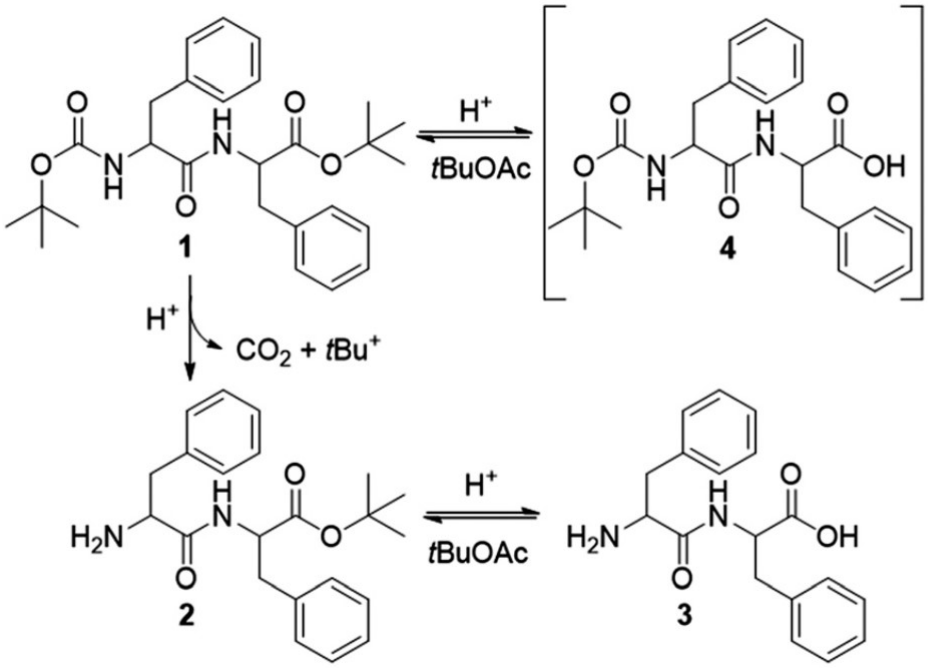

Figure 12: Structure of precursor gelator BocFFOtBu (**1**). Mechanism of the Boc-group selective deprotection under acidic conditions in the presence of the tert-butyl group. Gelation is dependent on the equilibrium of products **2** and **3**. A by product of the reaction is also dipeptide BocFF (**4**). Adapted with permission from Chevigny, R., Schirmer, J., Piras, C. C., Johansson, A., Kalenius, E., Smith, D. K., Pettersson, M., Sitsanidis, E. D. and Nissinen, M., Triggering a transient organogelation system in a chemically active solvent, Chemical Communications, 2021, 57, 10375–10378.[11]

The BocFFOtBu gel collapses almost instantly when in contact with water. This is due to the water re-esterificating the F-F portion of the molecule to F-FOtBu. However, under acidic conditions the gel does not break down due to the environmental prevention of re-esterification, making the gel stable in an acidic solution for approximately 1 week.[11]

BocFFOtBu and the formed derivatives FFOtBu and FF have aromatic moieties that may interact with graphene. Similarly to Fmoc-F, the gel would interact with graphene and be removed with hydrophilic solvents after the transfer. The gel could also be removed by heating, and collapsing the gel structure.

Results and discussion

In the results and discussion section, the experimental procedures are explained and the obtained results are presented.

Three types of gels were tested to replace PMMA polymer during the graphene transfer process. The interactions between graphene and the transfer gel were studied and compared to those between PMMA and graphene. The main goal of the project was to establish a new and modifiable transfer process using gels as the support layer and assess the interaction forces between graphene and the materials involved during transfer.

6 Graphene sample preperation

6.1 Production of Cu films

Cu(111) films were prepared using a modified method of David L. Miller[4] (section 2.1.1). Copper was vaporized on top of square 5x5 mm α-Al_2O_3(0001) sapphire substrates. The sapphire was cut to sample size and annealed in a Eurotherm 3216 PID oxidizing furnace at 1100 ℃ under O_2 atmosphere for 24 hours. Annealing polished the sapphire and removed any surface contamination. The quality of the substrates was assessed by optical microscopy. Copper was applied on the sapphire substrates using a BAL-TEC BAE 250 vacuum thin film deposition system. The substrates were attached to a Cu puck and placed in the system, where they were left to coat for 20 minutes. This treatment produced a 400-500 nm thick Cu(111) layer on the sapphire substrate. The copper chips were cooled down and removed from the system to proceed further with graphene synthesis. The samples were prepared by laboratory technician Olli Rissanen.

6.2 Graphene synthesis method

The synthesis of graphene was performed using a home-built GLS-1100Z MTI corporation graphene furnace (Figure 13). Control samples were annealed in the tube furnace under an atmosphere of 470 sccm of Ar (partial pressure of 1145,1 mbar) and 27-30 sccm of

hydrogen (partial pressure of 67,6 mbar) for 20 minutes. Graphene was synthesized under 4,7 sccm of 99% Ar and 1% CH_4 atmosphere (methane partial pressure of 11,3 mbar) for 20 minutes. Treatments were done under the temperature of 1050-1060 ℃. The samples were cooled in the tube furnace for 10 minutes prior to removal.

Figure 13: Home built GLS-1100Z MTI corporation graphene furnace.

6.3 Sample characterization

The samples were assessed initially using an Olympus BX51M (2008/2008) optical microscope to verify the condition before and after the transfer process.

To verify the presence of a graphene monolayer, the samples were analyzed using the Raman spectrometer Termo Fisher DXR Raman microscope at an excitation wavelength of 532 nm. The power of the beam was set at 4 mW and the pinhole at 50 μm.

The surface of the samples was further studied using a Bruker Dimension Icon (2016/2016) atomic force microscope. Bruker Scanasyst-Air silicon tips with nitride cantilever were used for the imaging.

6.4 Control samples

Control samples were transferred with the standard transfer process. After the graphene synthesis, a layer of PMMA was spin-coated on top of the graphene/Cu/sapphire chip in 4000 rpm with Laurell WS-650-23 spin coater. The PMMA was left to dry for 15 minutes. The chips were placed in an etching solution (APS 0.5 M) and left for 16 hours. After the etching was finished, The PMMA/graphene layer was moved through 5 water

vials and 1 HCl (1 M) vial to clean the excess APS and other possible residues. The PMMA/graphene layer was transferred to the final SiO_2 substrate and the PMMA layer was removed by dilution for 15 minutes in both acetone and isopropanol solutions. The final cleaning phase was done by annealing the substrate in a tube furnace at 300 ℃ under Ar (partial pressure of 1145,1 mbar) and H_2 (partial pressure of 67,6 mbar) atmosphere for 3 hours. After the annealing, clear residues of PMMA layer were observed, which is undesirable for any further use of the samples. Optical images of the two control samples are given in figure 14

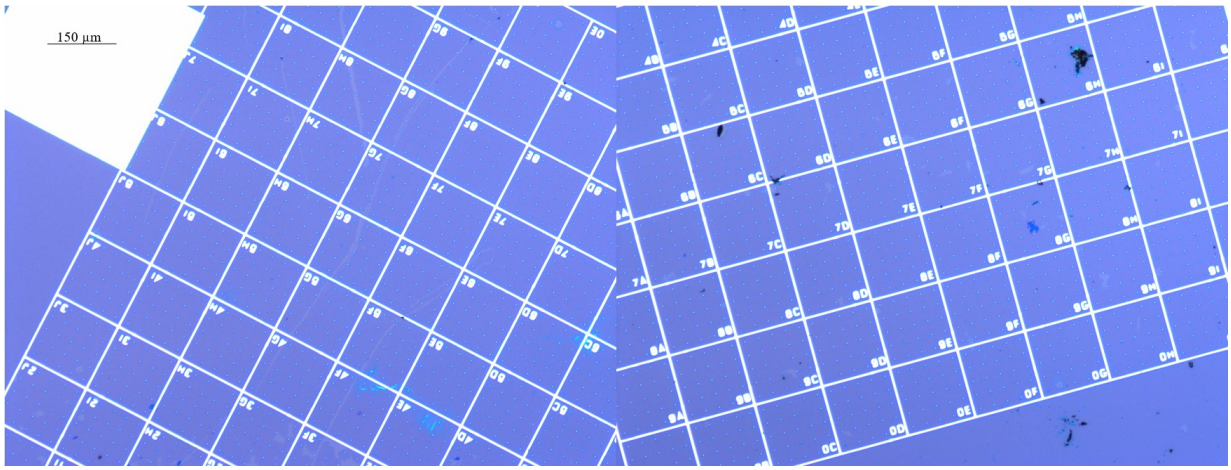

Figure 14: Optical images of two control samples after graphene transfer.

Raman spectra were measured from the control samples (Figure 15). The grey spectrum is taken from the clean part of the samples. The red spectrum shows PMMA contaminated sample. PMMA residue increases the background of the spectrum and width of the 2D band.

Samples were imaged also by AFM to study the adhesion forces between graphene, silicone, and the contaminants. An AFM image from the control sample 1 is shown in Figure 16. All of the measured AFM images had low resolution and distortions. This is due to the AFM tips used in this study, which were old and possibly damaged. During the experimental work, no new or clean AFM tips were available, therefore AFM imaging needs to be repeated.

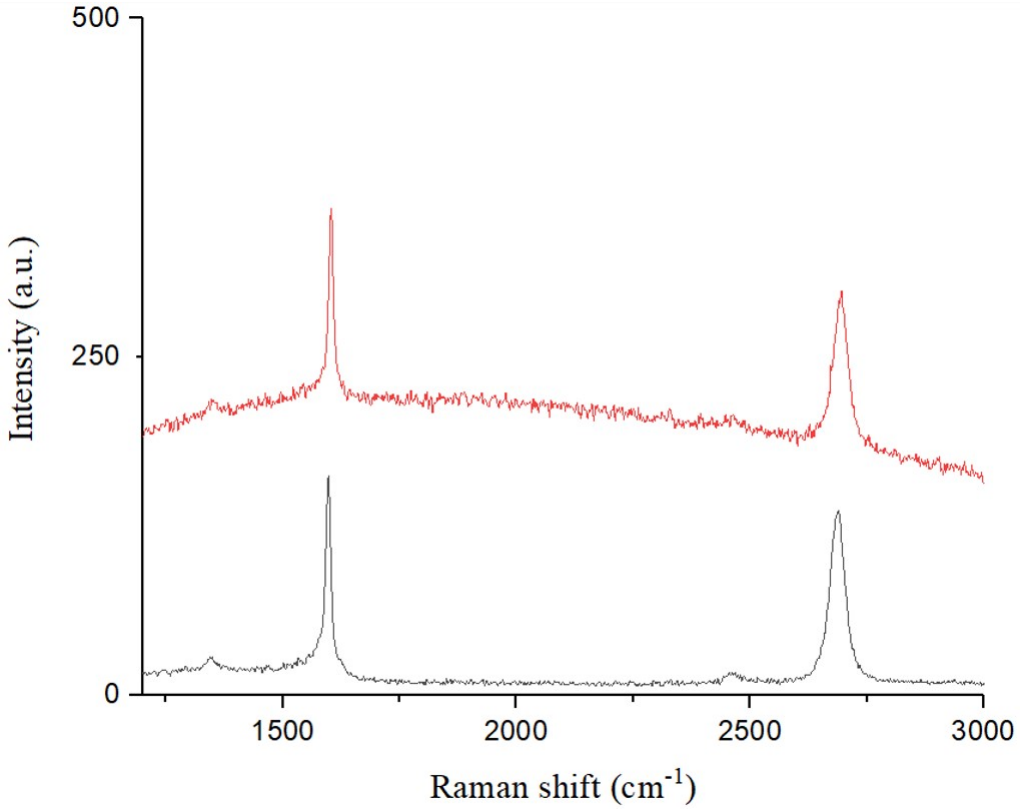

Figure 15: Raman spectra of the control samples. Clean graphene (grey) and PMMA-contaminated graphene (red).

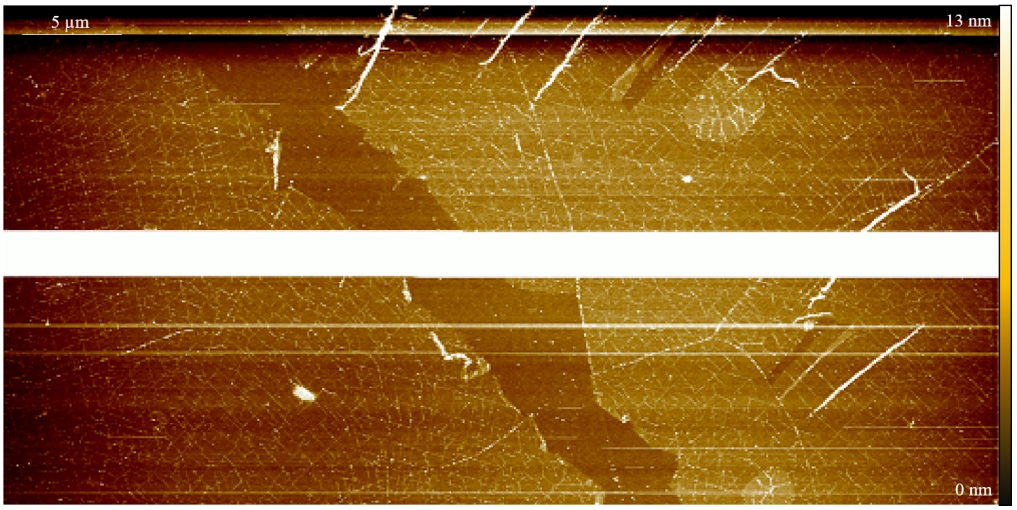

Figure 16: AFM figure of the control sample 1.

7 Gel transfer study

7.1 Gel stability studies

The studied gels had to meet specific requirements based on those applied during the graphene transfer method. Specifically, they should interact with graphene, be stable and withstand pH changes, and be easily removed. To meet the first requirement, a gel had to form weaker interactions with graphene than with unoxidized silicone and water. Graphene does not interact strongly with small polar molecules like water. This means if the gel could develop interactions with the graphene monolayer and survive the etching, then the transfer process would be successful.

The second requirement was the most challenging. The stability of three different gels was tested, HA, Fmoc-F, and BocFFOtBu. For each gel, three vials were prepared at different concentrations, of which one was the control sample. The second vial was placed in the fridge with 4 ml of added water on the gel's surface and the third was placed in the fridge with 4 ml of added APS solution (0.5 M). The gels were stored therefore under the simulated etching conditions, at a temperature of 4 ℃ for 16 hours.

HA gel was chosen due to its known biocompatibility and therefore there would be no need to be removed from the graphene surface. Indeed, human cells use it as a nutrient while it is one of the main components of the extracellular matrix in brain tissue.(section 5.9.1) HA gels were prepared by mixing hyaluronic acid (HA, 91%, AlfaAesar) with 1-(3-Dimethylaminopropyl)-3-ethylcarbondiimide hydrochloride(EDCI, 98%, AlfaAesar) and adipic dihydrazide (ADH, 97%, AlfaAesar). All compounds were diluted in water separately and mixed thereafter. The composition of the gel was constant at 80% of HA, 10% of EDCI, and ADH. Gelation was triggered by the addition of a hydrochloric acidic solution (HCl, 1 M). The vials were then left for 12 hours at room temperature to allow gelation to occur.

N-[(9H-Fluoren-9-ylmethoxy)-carbonyl]-L-phenylalanine (Fmoc-F-OH, 98%, TCI) was mixed with PBS solution by sonication. The suspension was heated for 30 minutes at 80 ℃. The vials were left at room temperature for 12 hours undisturbed for gelation to occur. Fmoc-F gels were prepared at concentrations of 2.0, 5.0 and 10 mg/ml.

The dipeptide *N*-tert-butyloxycarbonyl (Boc)–L-phenylalanyl–L-phenylalanine tert-butyl ester (BocFFOtBu) was mixed with tert-butyl acetate (tBuOAc) solvent. The solution was sonicated until a clear solution was obtained and 2,7 μl of saturated sulfuric acid (H_2SO_4, 95-97%, Fluka) was added. The vials were then left for 24 hours at room temperature to allow gelation to occur.

Stability tests were also performed on HA gel films. The films were prepared by the solvent cast method where a HA solution was poured into a 2cmx2cm mold. Then HCl was added to initiate gelation. The gels were left to dry for 48 hours at room temperature and the formed films were placed in an APS solution for 12 hours. The drying HA gels in the mold towards gel films are shown in figure 17

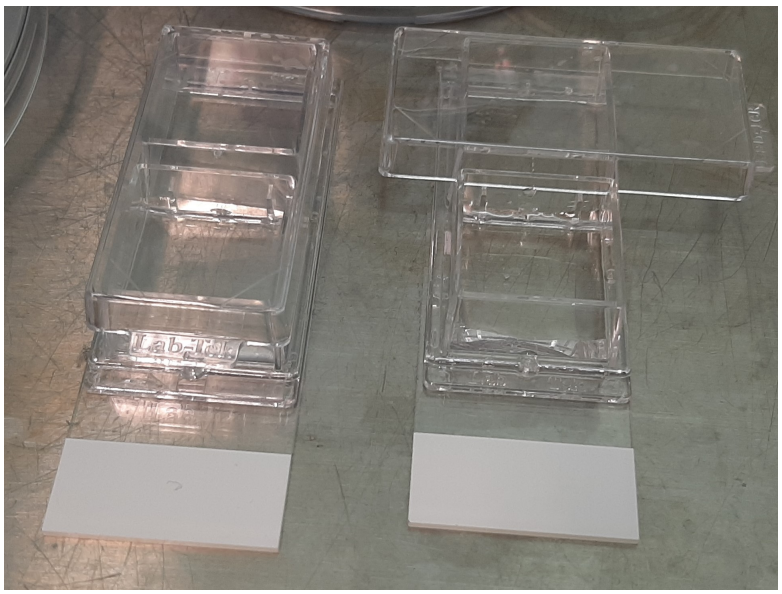

Figure 17: Preparation of HA gel films by the solvent cast method using glass chamber molds.

7.1.1 Gel stability results

HA was able to withstand the etching conditions both at the gel and film forms. The gel swelled in water and APS but remained stable, as checked by the vial inversion method (Figure 18).

The Fmoc-F gel was not stable under the experimental conditions. The gels had a soft structure in the APS solution, while white flocculent parts of the gel and aggregates

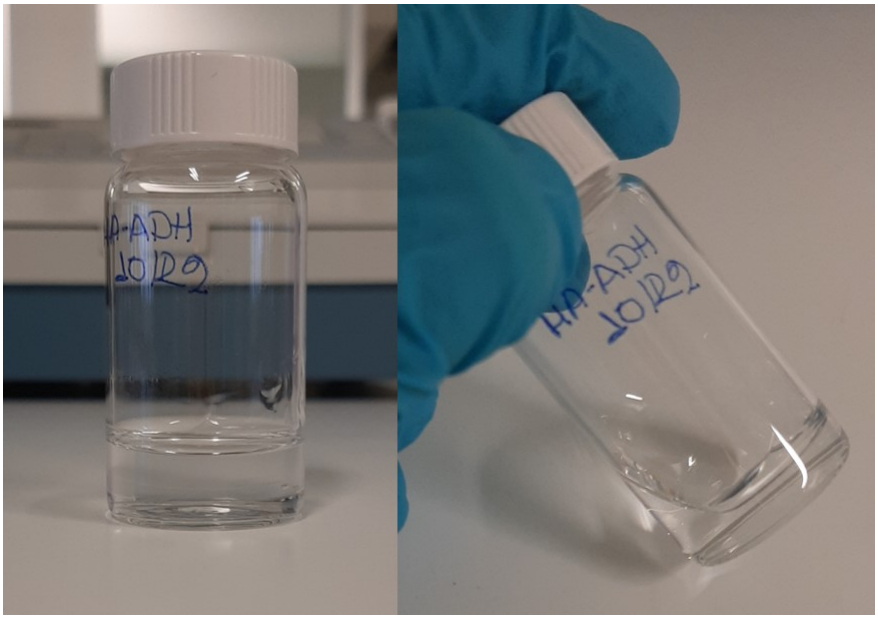

Figure 18: A HA gel sample after the stability test. The HA gel is covered in APS as to imitate the etching conditions (left). The tilted vial shows the gel intact at the bottom (right).

were floating in the APS solution after 16 hours. All Fmoc-F gel samples gave the same outcome (Figure 19).

It is of note that at a higher concentration of the gel, the forming wight aggregates formed (precipitation of Fmoc-F) instead of a flocculent gel. Lower concentrations formed rather flocculent gels and no precipitation was observed. The experiment was repeated at concentrations of 1.0, 2.0, 3.0, and 4.0 mg/ml of Fmoc-F. White flocculent gels were formed (Figure 20) and the concentration effect was evident as above. At the concentrations of 3.0 and 4.0 mg/ml the gels were weaker (multiple blobs of flocculent gel were formed) compared to the concentration of 1.0 and 2.0 mg/ml (two faces are observed). This collapse of the original gel can be explained by the solvent exchange process. The APS solution in the etching process dilutes the encapsulated PBS in the gel. This results in a softer material of Fmoc-F. Based on the obtained results, the 2 mg/ml flocculent gel was used in the transfer experiment. Flocculent gels that had been through the etching conditions were used, because the solvent exchange occur again and shrink the gel further. If the solvent exchange would happen during the etching process, graphene would ripple and fold. The lower concentration Fmoc-F flocculent gels were stable in the APS solution over a month.

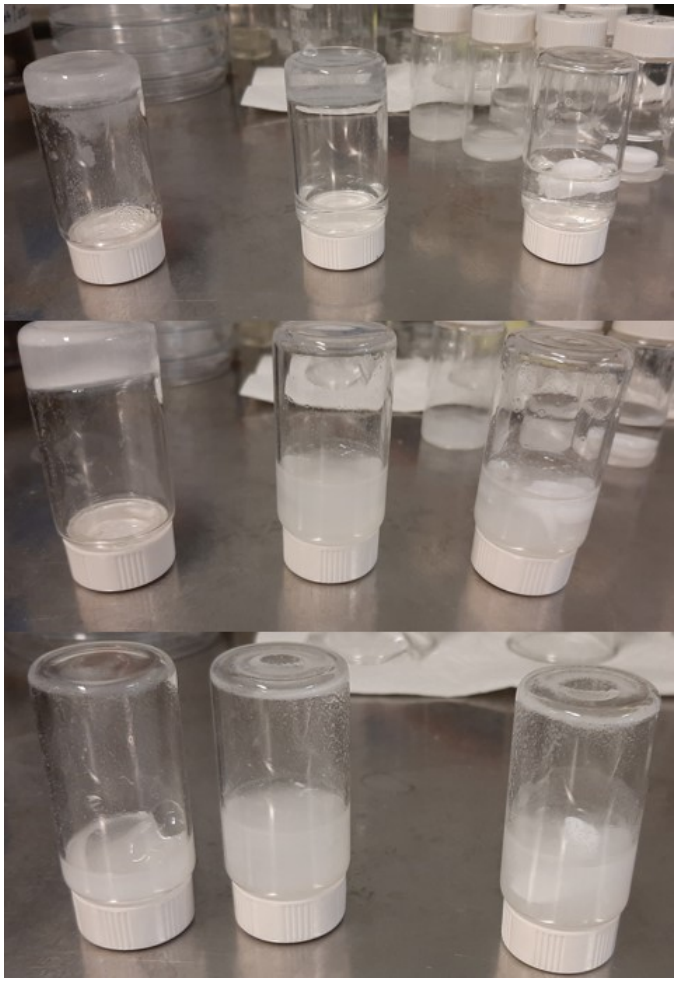

Figure 19: Fmoc-F gels after the stability test. The concentrations from top to bottom are 2.0, 5.0, and 10 mg/ml. The controls for each concentration are on the left. Middle vials were filled with water and the right vials were with APS solution.

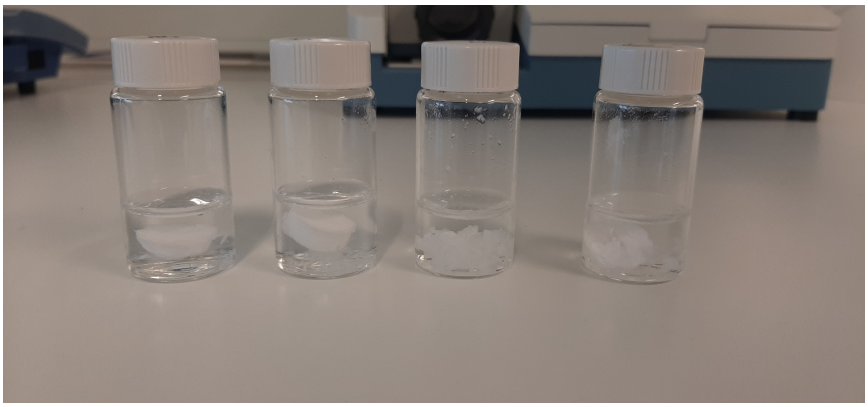

Figure 20: Fmoc-F gels after the stability trials at concentrations of 1.0, 2.0, 3.0, and 4.0 mg/ml (left to right).

BocFFOtBu gels did not pass the etchant test. All tested gels dissolved in water and created a foamy liquid in APS solution (Figure 21). As the literature predicted in section

5.9.3[11], the gel did not dissolve completely to acid. The gel could stay more stable in a more acidic environment.

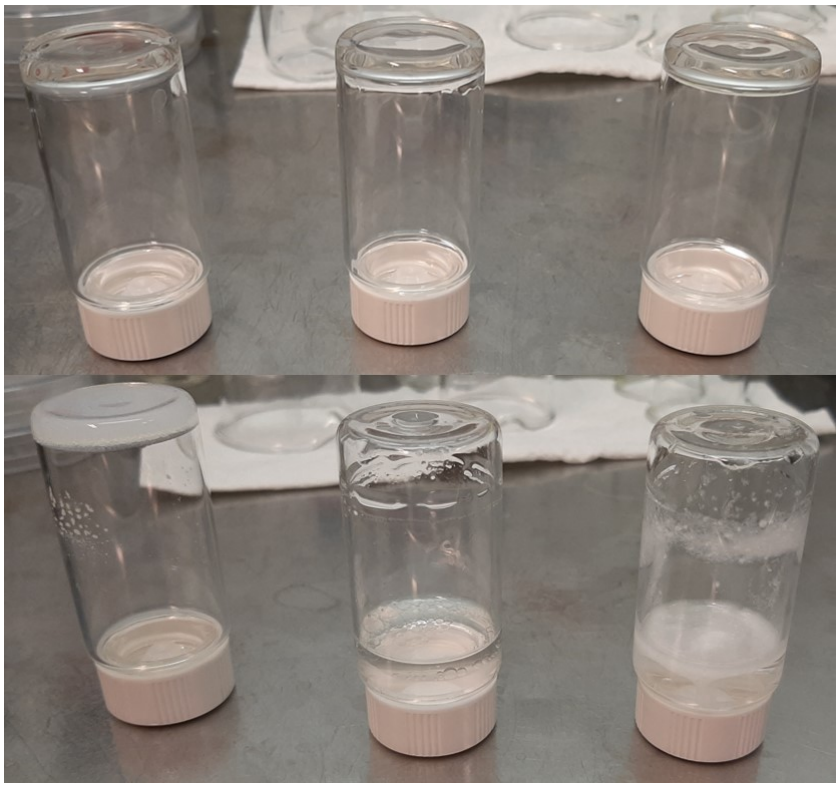

Figure 21: BocFFOtBu gels before (upper) and after (lower) the stability test. Control gel (left), gel tested with water (middle), gel tested with APS (right).

7.2 Gel thickness

HA-gel was spin-coated on top of a cleaned sapphire chip at speeds of 500 to 6000 rounds per minute (rpm). The sapphire chips were cleaned with water, acetone, and isopropanol. The HA-gel solution was prepared separately in a vial by adding 7.6 μl of 1 M HCl to initiate gelation and one drop was pipetted on top of the sapphire. The sapphire/gel interface was analyzed by AFM to assess the thickness of the formed gel layer.

The effect of spin coating the gel layer is shown in figure 22. The 500 and 100 rpm formed a thick and sticky layer of gel. The AFM data could not be obtained because of the large difference in height and issues with the AFM tips (section 6.4). At a higher spin, the gel forms a very thin layer that could be damaged during the etching process. During the standard process, the spin coating of PMMA produces on average around 400 nm thick layer.

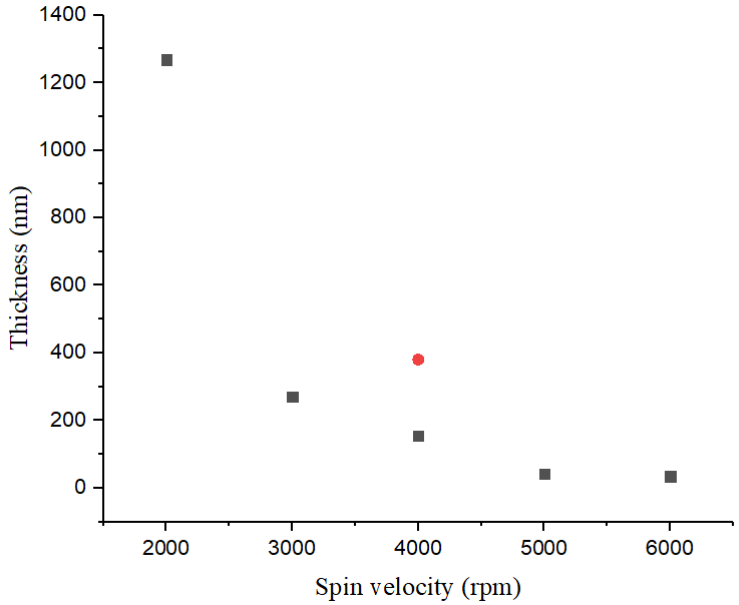

Figure 22: Gel thickness relative to spin-coating. HA gel (black squares), control PMMA layer (red dot).

As the gel forms a thinner layer at 4000 rpm, it could leave fewer residues on top of the graphene when it's removed. It was decided to study the spin coating of gels at 500 and 4000 rpm. These spinning velocities would help to deduce the optimal gel thickness for the transfer process.

7.3 Transfer

The first two transfer experiments were performed using a 10 mg/ml HA gel on top of the graphene/Cu/sapphire chip which was spin-coated. For the first transfer attempt, one drop of the gel was applied on top of the chip as it was still viscous and was spun at 4000 rpm. After spin coating, a second drop of the gel was added on top of the surface and spin-coated for a second time to ensure the presence of a gel layer. The chip was then etched using a 0.22 M APS solution overnight. After the etching, the gel was moved from the etching vial to the water vial to remove excess acid. From the water vial, the gel was transferred to the final SiO_2 substrate and then analyzed with an optical microscope, before moving to AFM and Raman measurements.

For the second transfer attempt, the gel was applied on top of the chip immediately after it formed (one minute after the addition of HCl). The chip was then spin-coated at 4000

rps, as seen in Figure 23. The chip was moved to the etching process and transferred to the final substrate in the same way as the first samples.

Figure 23: Second transfer attempt by the spin coating of HA gel on the chip. The chip/gel system before (left) and after spin-coating (right).

At a third attempt, the gel formed overnight on the chip surface without spin coating. To ensure no drying of the gel during the gelation process, the chip was placed in a chamber saturated with moisture. A beaker was placed upside down in a larger beaker filled with water and the chip was placed on top to allow gelation to occur. A piece of filter paper was stuck on the wall of the larger beaker to allow saturation in moisture and the chamber was sealed with a watch glass (Figure 24). The gel was left for 24 hours before the chip was transferred to APS solution for 12 hours.

Figure 24: Third experimental attempt. A glass chamber set up without the watch class. The left and middle figures show the chip covered by the gel immediately after the gel application and the right figure shows the chip and the gel after 24 hours.

At a fourth attempt, a HA film was used. A piece of dry film was cut at the size of the chip and applied on its surface. A drop of water was added to the dry film to ensure it will attach to the chip's surface. The film was left to dry overnight (Figure 25) and the chip was transferred to APS solution for 12 hours.

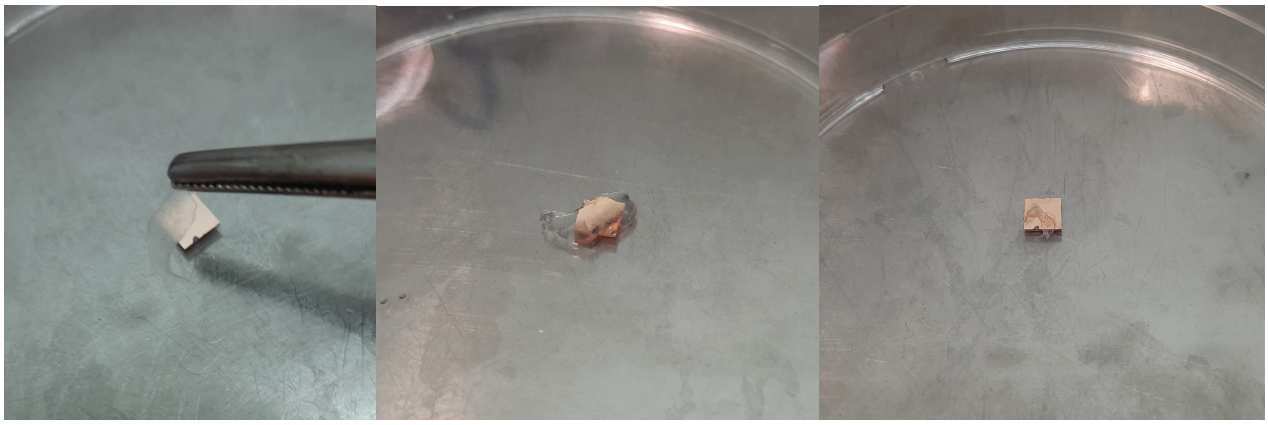

Figure 25: HA gel film transfer. On the left, is the application of a dry gel film. In the middle, the wet film is now attached to the top of the chip. On the right, the dried film has still attached to the top of the chip.

The fifth and sixth transfer attempts were performed using copper film as the growth platform. In the fifth trial, the gel was applied directly on top of the copper film and moved to the etchant directly. In the sixth trial, the gel was left to dry on top of the film for approximately 24 hours.

The seventh and eighth experimental trials were also performed using copper film on which a HA gel film was applied. The gel films were prepared by the solvent cast method (see section 7.1). During the seventh trial, the film was placed on top of graphene without any solvent added thereafter. In the eighth trial, the film was added on top of the graphene and a couple of water drops were added to ensure its attachment. The foil/gel system was left for 24 hours before its transfer to the etchant.

The transfer was tested using also the soft Fmoc-F flocculent gel (section 7.1.1). The flocculent gel at a concentration of 2 mg/ml was created during the stability testing of Fmoc-F gels. The formed flocculent gel was removed from the vial using pincers and was cut into smaller pieces with a spatula. Before the etching, a blob of flocculent gel was placed on top of the graphene/Cu/silicone chip and was let to dry for half an hour. The chip was then placed in an APS solution overnight.

7.3.1 Transfer experiments

The first HA gel transfer attempt successfully overcame the etching procedure and HA gel was transferred to the final substrate. Optical images before and after etching are shown in Figure 26. A large area of the gel had been transferred to the final substrate. The gel was not homogeneous, as the thicker regions were clearly visible after the transfer process, while graphene was not visible in large quantities.

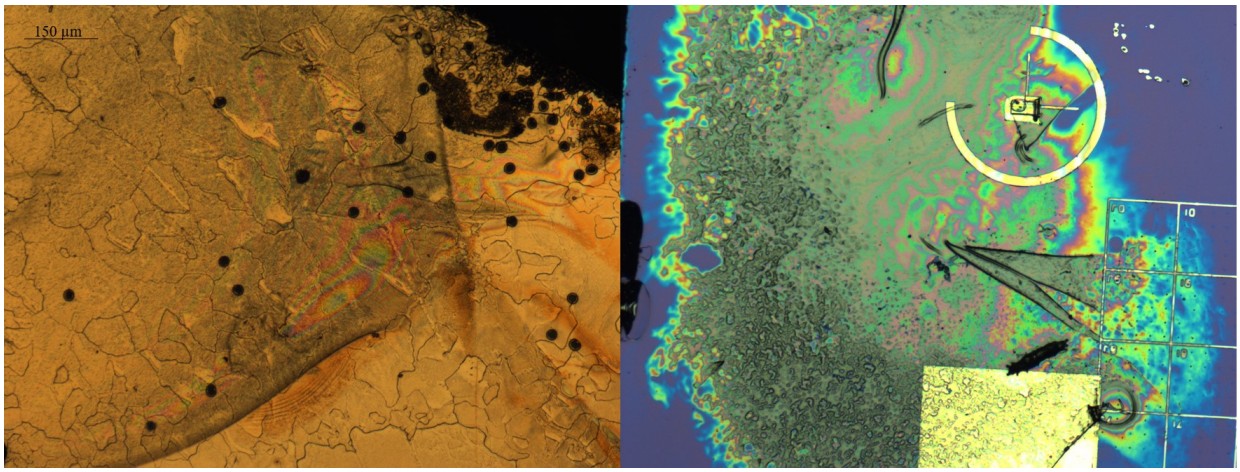

Figure 26: First gel transfer attempt. The surface of the chip before (left) and after (right) etching at 50x magnification.

After a closer inspection with the optical microscope, the gel showed some darker spots that resembled graphene. These spots were confirmed to be graphene by Raman spectroscopy. The optical images of graphene and the measured Raman spectra are given in Figure 27. This confirmed that the HA gel can survive the etching process and transfer some quantities of graphene. However, graphene was not transferred in usable quantities.

Compared to the Raman spectrum from literature (section 7.1 Figure 9), the HA gel Raman spectrum does not show significant activity in the Raman shift area characteristic to HA. With this knowledge, the rest of the HA gel transfers were studied with Raman, and the existence of graphene in the sample was confirmed before the attempts of gel removal. If the Raman spectrum was similar to the pure gel one (Figure 27.a) the gel removal process was not attempted.

At the second transfer attempt, the attachment of the HA gel on top of the graphene was confirmed with an optical microscope after the spin coating (section 7.3). Optical images of the graphene/Cu layer before and after the gel application are given in Figure

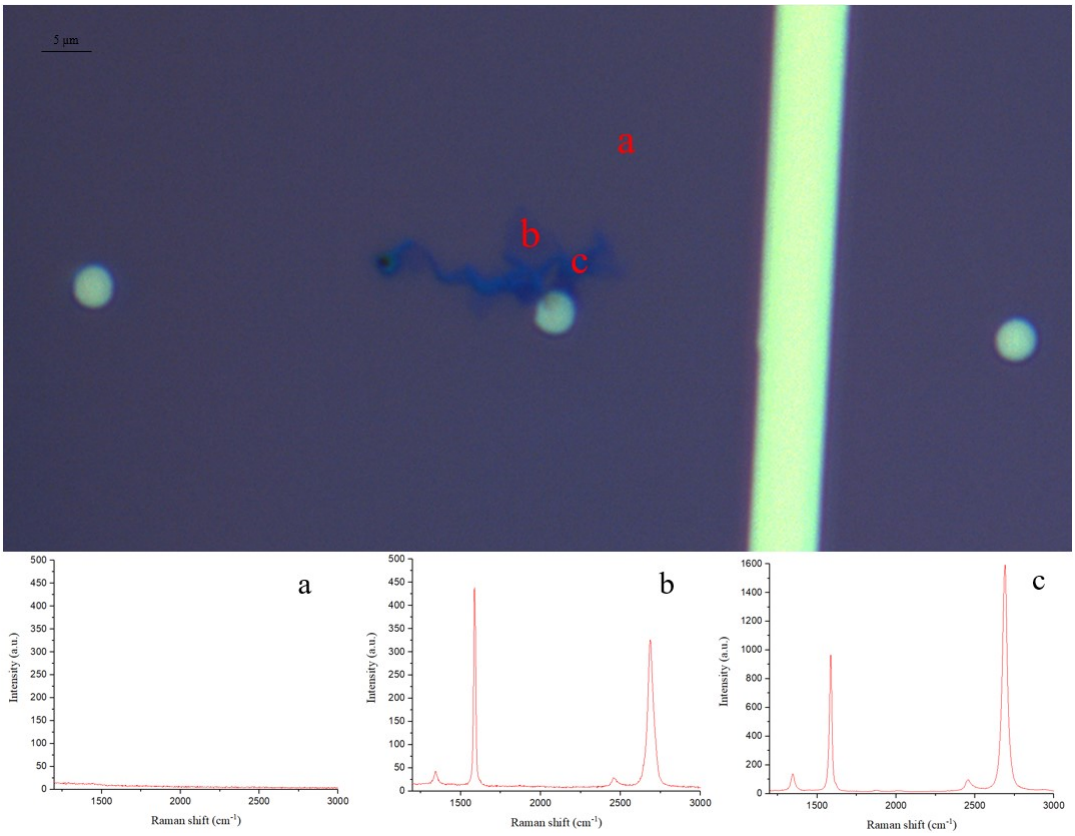

Figure 27: Transferred graphene from the first experimental attempt. The Raman spectra from different areas (a, b, and c) are seen below the optical images. Thin layer of gel (a), single layer graphene (b), rolled graphene (c).

28. The attached gel made the surface darker and the layer was recognizable from the added structures on the surface. The HA gel did not survive the etching process and no gel or graphene was recovered after etching. By this attempt, it was evident that it is preferable to allow the gel to form on top of graphene, rather than in a separate vial and transferred afterward.

The rest of the transfer attempts showed similar results. The transferred graphene was either too small in size to be used further or it was damaged to the point of not being able to be used or cleaned. This can be evident in Figure 29, showing the result of the sixth attempt. In the image, the broken gel film and other contamination are seen. There is not visible layer of graphene other than the damaged gel.

In all trials, a very small area of graphene or nothing was transferred. The reason for this could be that between graphene and gel is not strong enough thus it does not transfer. From the structure of hyaluronic acid (section 5.9.1, Figure 8) multiple positions to form hydrogen bonds are seen. This is the reason why HA dissolves in water. In the etching

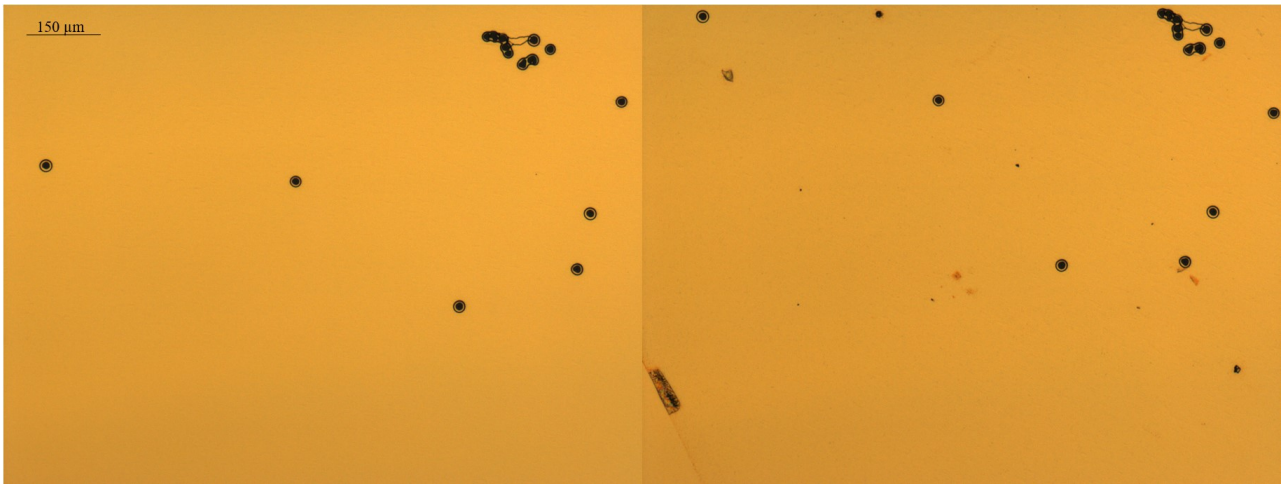

Figure 28: The second transfer attempt for the HA gel attachment at 50x magnification. Before gel application on the left, after gel application on the right.

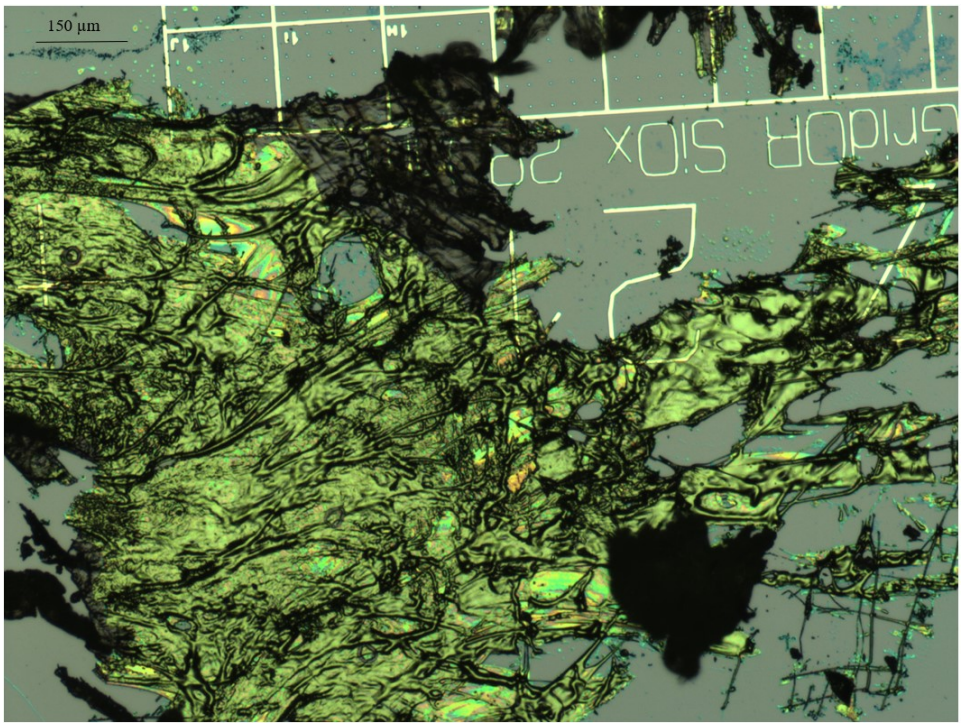

Figure 29: Transfer results of the sixth attempt. Visible parts of broken gel and other contamination are shown.

solution, there is a 0.5 mol/l concentration of APS in water. This suggests that the gel and the corresponding film rather interact with the water in the etching solution more than with graphene. The gel absorbs water, which is trapped between the gel layer and graphene, overcoming the formed interactions that are formed when the gel is applied. This leads to the detachment of graphene, which is destroyed by the etching solution. Gel/graphene interactions are present to some extent, which is evident by the

first experimental attempt. Graphene does not interact with water or the gel, thus the sapphire chip, which had the copper layer on top of it, was assessed under an optical microscope. To compare our data to a control sample, a sapphire chip that had just been used at the standard transfer procedure was studied (Figure 30).

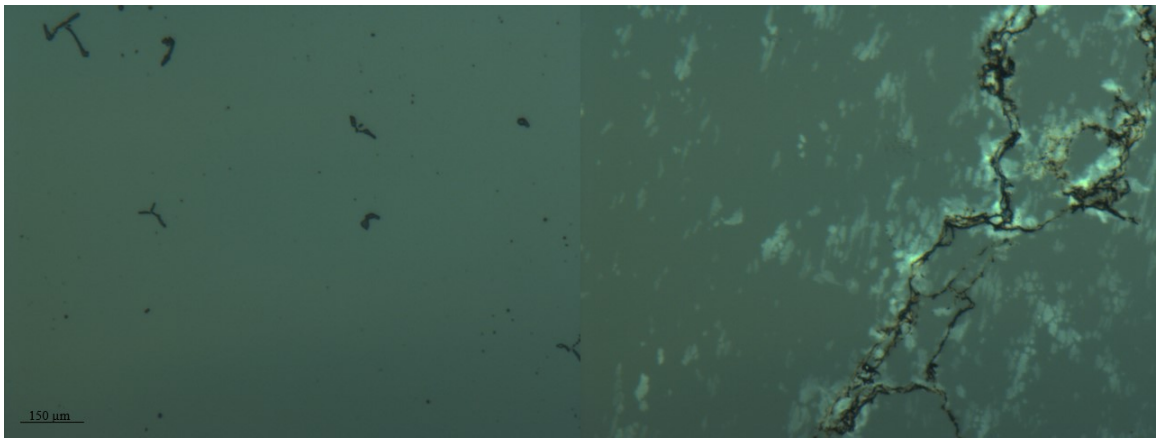

Figure 30: A sapphire chip after the standard transfer (left) and a chip used for the gel transfer (right).

The comparison shows that the white areas on the sapphire (right image, Figure 30) are not present after the standard transfer procedure. To confirm if these spots were graphene, Raman spectra were measured from all the chips (Figure 31). The characteristic Raman peaks of multilayer carbon are seen. This means, that graphene interacts with the sapphire chip more than the gel. Therefore, all the sapphire chips from all experimental trials were studied to investigate if graphene is attached to the sapphire rather than the gel. Indeed, all chips showed similar behavior. This supports our hypothesis, as the trapped water between the gel and graphene repels graphene down on the sapphire. The graphene monolayer is pushed down to the sapphire during etching while water also starts breaking graphene and rolling it.

The interaction between graphene and HA has been documented in literature[13,50] and the first transfer attempt was successful, however, only a small area of graphene was transferred. This research could be expanded by researching optional solvents other than water for gel formation. The challenge in this research is the hydrophilic nature of HA (section 5.9.1 Figure 8). To overcome challenges as such, a solvent less polar to water could be used to form HA gel and support the gel/graphene interaction during the etching process.

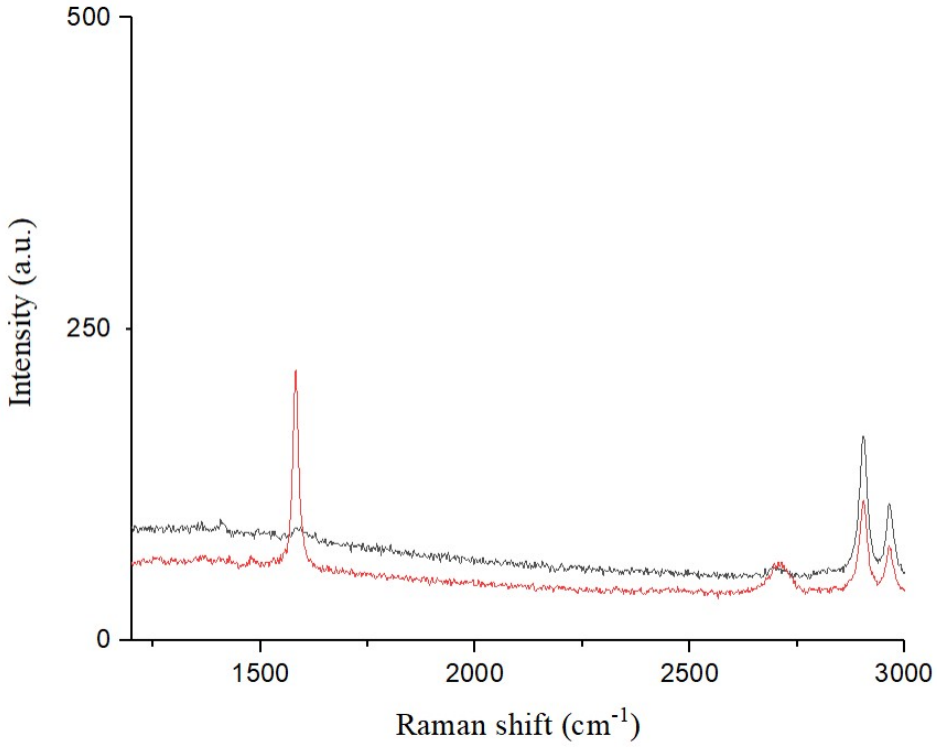

Figure 31: Raman spectra of sapphire chips. Grey is the spectrum of clean sapphire and red is the spectrum of gel transfer sapphire.

The Fmoc-F gel transfer was not successful either. The Fmoc-F gel was not stable enough during the etching process and broke into smaller pieces. No graphene was retrieved from this experiment. Fmoc-F is amphiphilic in nature meaning that the corresponding gel could interact with graphene. However, the formed flocculent gel was not stable enough to withstand the etching procedure.

Even though this trial failed, Fmoc-F has the potential as a transfer gel. Indeed, Fmoc-F gels withstand the etching conditions twice. This means that the gel does not interact with water or APS solution. The intermolecular forces are not strong enough to keep the Fmoc-F flocculent gel intact, to some degree. Secondly, the amphiphilic nature of Fmoc-F allows the use of other solvents that would form more stable gels. A hydrophobic gel (formed using a polar organic solvent) would not interact with water during the etching procedure. A summary of the outcome of the transfer trials is given below in Table 2.

Table 2. Summarized results of gel transfer experiments

Experiment	Pre-etching treatment	Result
HA 1	A viscous HA gel was applied twice on graphene while the gel was forming. the chip was spin-coated at 4000 rps after each gel addition.	Small amount of graphene was transferred.
HA 2	the gel formed and was applied afterward on graphene and spin-coated at 4000 rpm.	Gel broke down
HA 3	The gel formed on top of Cu/graphene chip overnight in a saturated, moist chamber.	Gel broke down.
HA 4	A gel film was applied on top of the Cu/graphene chip. A drop of water was added and the chip was left to dry overnight.	Gel broke down.
HA 5	The gel was applied on the Cu film following directly etching.	Gel broke down.
HA 6	Á gel was applied on Cu film and was left to dry for 12 hours before etching.	The gel was transferred, traces of possible graphene.
HA 7	A gel film was applied on Cu film and moved to etchant.	Gel broke down.
HA 8	A gel film was added on top of Cu film with couple of water drops. The film was dried for 24 hours.	Gel broke down.
Fmoc-F	The gel was applied on top of Cu/graphene chip and was left to dry for half an hour.	Gel broke down.

7.3.2 Transferred graphene quantity

The transfer experiments did not produce enough quantity of graphene to be studied. Only the first trial yielded graphene that could be imaged by Raman spectroscopy (Figure 27).

7.4 Gel removal

Since there was not enough graphene recovered, gel removal was not performed. The gel removal would have been performed with the following protocol: each gel was to be washed with its solvent, that is water for HA gels, PBS solution for the Fmoc-F gels, and tBuOAc solvent for the BocFFOtBu gels. The silicone/graphene/gel chips would have been submerged in the corresponding gel solvents for 20 minutes while the stability of each chip would have been studied at 5-minute intervals with an optical microscope.

7.5 Adhesion energy of the materials

The adhesion energies between the copper, copper/graphene, copper/graphene/PMMA, silicone/graphene/PMMA, silicone/graphene, and silicone/graphene/gel chips were studied to understand the adhesion forces of the materials. Equations 5 and 6 (section 3.2.2) are used to obtain the adhesion energy of the AFM data. The adhesion data would allow the comparison of molecular interaction forces between the gel and PMMA transfer.

7.5.1 Adhesion energy calculations

The adhesion of the substrates was studied using AFM. The average adhesion energy of the measured area was determined using Gwyddion software. Studied areas were taken so that there was minimal distortion in the image. An example of the adhesion measurement is shown in Figure 32.

The adhesion force was taken and it was applied to equation 6. This value was also added to the equation. This produced the adhesion work (W) that can be added to equation 7 to get the adhesion energy. This gate the adhesion energy in Joules, and it was changed to electron volts (eV). The extracted adhesion energy for the graphene/Cu interface was around 0.4 μeV. These calculations were also affected by the AFM problems described in section 6.4 and thus the results are not reliable.

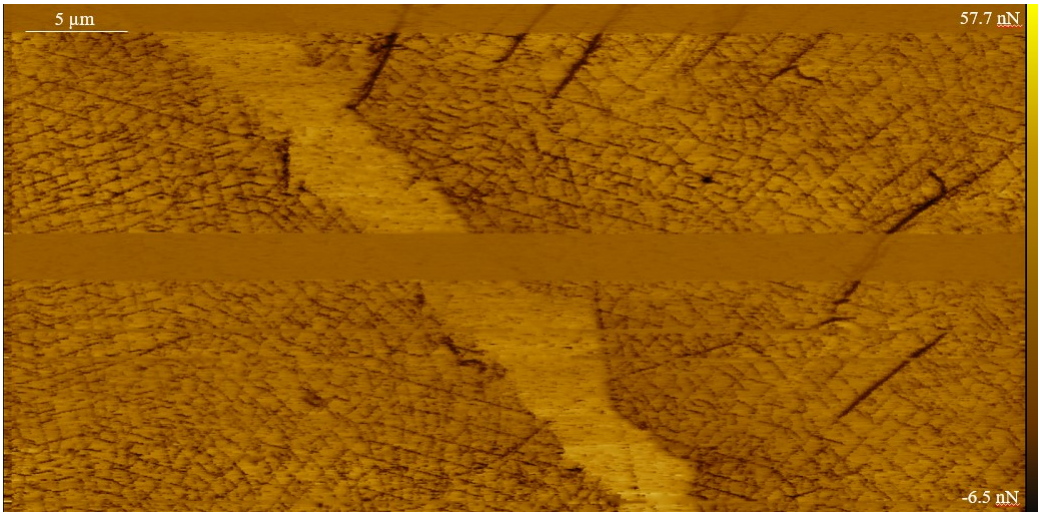

Figure 32: Adhesion energy figure from the control sample seen in figure 16.

8 Hyaluronic acid films

HA was dissolved in water at a concentration of 10 mg/ml. The solution was placed in a glass chamber mold and was left overnight (Figure 33). When water was evaporated, the film was tested for its stability by heating, with and without water at temperatures 20-40 ℃ at 5 ℃ intervals using a block heater. Additionally, the Raman spectrum of the HA film was measured (Figure 36).

Figure 33: Preparation of HA films in water (left) and anisole (right).

Two extra films were prepared in anisole (Sigma Aldrich, 99%) as a solvent. The film stability experiments were repeated and the solubility in anisole was also tested, as well as that in isopropanol and acetone. The stability experiment set up for the water temperature test is shown in Figure 34.

Figure 34: Stability test of the films by heating. HA-anisole film (up) and HA-water film (down). Films heated in water (left) and without water (right).

8.1 Properties of films

The produced films had visual differences depending on the solvent. The HA/water film was very thin, transparent, and slightly elastic. The HA/anisole film was much stiffer and harder than the water film. It didn't bend and it was not transparent. In Figure 35 the difference between the film and gel film is given. The properties of the produced films were studied at several temperatures. The observed changes in the films by temperature are summarized in Table 3. The HA/water film was quickly dissolved in water while heating. All other films remained stable during the heating process.

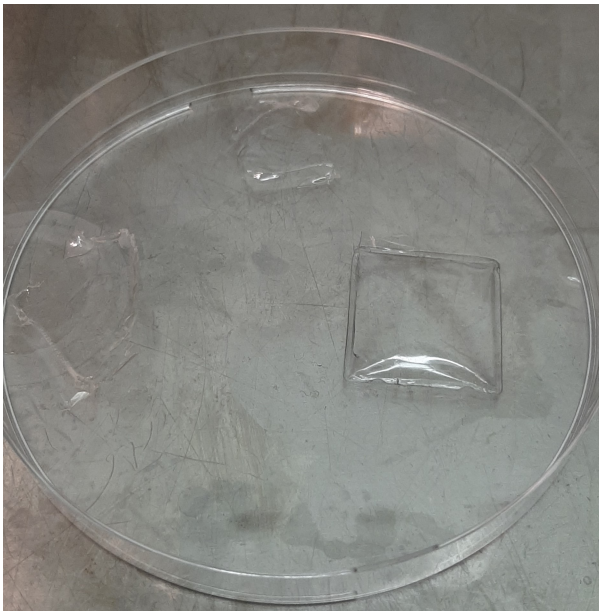

Figure 35: Differences in HA gel and HA film. HA gel films (left and middle), HA film made in water solution (right).

Table 3: Film stability trials at several temperatures.

Temperature (℃)	HA/water film	in H_2O	HA/anisol film	in H_2O
20	s	s	s	s
25	s	m	s	s
30	s	m	s	s
35	s	m	s	s
40	s	m	s	s

s = solid, m = melted

The HA/anisole film was soluble in anisole. The film was stable in boiling water, boiling acetone, and boiling isopropanol. The Raman spectra of the films are given in Figure 36. The Raman spectrum of the HA/water film is qualitatively different from that reported in the literature (section 5.9.1 Figure 9). The peaks 8 and 9 are visible approximately at 3000 cm^{-1}. There is a clear absence of peak 7, but weak peaks 4/5/6 can be detected below 1500 cm^{-1}.In addition, water is not peaks are not active in Raman.[58] Similar observations can be made for the HA/anisole 10 mg/ml film. No peaks can be appointed to anisole.[59] The 40 mg/ml HA-anisole film showed a completely different behavior compared to other films. The spectrum has some similar activity around 3000 cm^{-1} as in other spectra, but the background is much higher. The spectrum does not resemble those of HA or anisole.

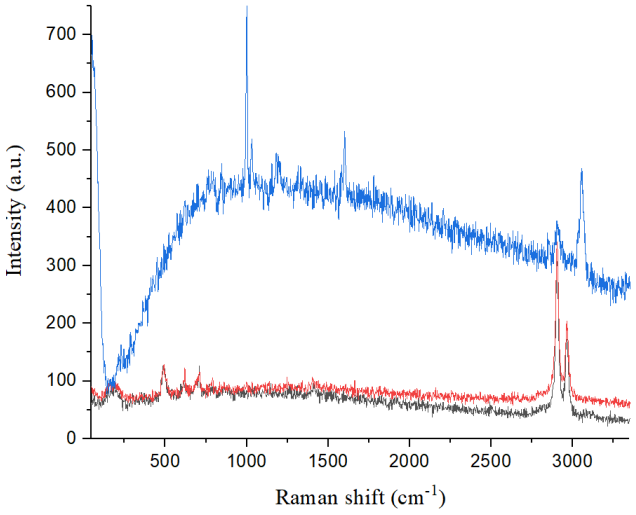

Figure 36: Raman spectra of the 10 mg/ml HA film prepared in water (black), 10 mg/ml of HA in anisol (red) and 40 mg/ml of HA in anisol (blue).

8.2 Graphene transfer using films

The transfer of graphene by films was tested by adding a piece of film on top of the graphene/copper chip. At the first attempt, the film was placed on top of the chip. At the second attempt, a drop of solvent, water, or anisole, was pipetted on top of the film after its placement on top of the Cu/graphene chip. The solvent was left to evaporate overnight. The chips were placed in the etchant after the solvent had evaporated. The transfer process was performed as described in section 6.4.

8.3 Film assisted transfer

After testing both methods of transfer, neither of the films was able to transfer graphene. The films either did not survive the etching process or didn't attach to graphene.

9 Computational work

Computational work was performed as part of the course project in course KEMS409 Material modeling. The computational work was performed in the chemistry department cluster. Computational work was done to visualize the adhesion energy differences between copper and graphene. The results would be compared to the experimental mea-

surements of adhesion with AFM. Materials modeling and calculations were done using Grid-based Projector-Augmented Wave (GPAW), which is based on Python language. To visualize the forming structures, the graphical interface for the GPAW and Atomic Simulation Environment (ASE) were used.[60,61] Cu(111) surface was modeled and optimized, using reported calculations to metallic surfaces optimization[62], to the orientation of crystal structure 111 by testing different k-point values. Two bottom layers of the optimized bulk structure were fixed to stimulate multiple layers of graphene and the forming slab structure was optimized by itself with the same k-point values.

The graphene was optimized using graphite optimization script as a base and removing one layer from optimized graphite to create the graphene. The produced structures were combined and optimized. The adhesion energy between the structures was calculated from optimized structure energies. Optimized structures were combined into the same trajectory file and optimized to find the internal energy of the system. The k points, that determine the calculation accuracy, used in the graphene surface optimization were (4,4,1). The graphene lattice constant (a) was altered to be 2.445 Å to align the graphene with the (111) metal surface, as it has shown to be a good approximation.[63]

To determine the molecular interactions in the system, the Van der Waals density functional (vdW-DF) was used in the calculation, and the Strain filter was used to determine lattice vectors. Calculations were run in a vacuum cube with a side length of 14 Å.[64,65,66] Calculations had a cut-off energy of 0.05 to optimize the structure in minimal energy. Determination of adhesion energy was done by comparing the optimized graphene and copper energies to the combined system energy. The adhesion energy can be calculated from the energy difference of the structures.[64,66]

$$\gamma_{\mathrm{A}} = \gamma_{\mathrm{CuG}} - \gamma_{\mathrm{Cu}} - \gamma_{\mathrm{G}} \tag{15}$$

In the equation, γ represents the energy, lower index G graphene, lower index Cu copper, and lower index A adhesion.

9.1 Computational results

To optimize Cu(111) structure, the tested k-points and their energies can be seen in Table 4 and the evolution of the energies is shown in Figure 37.

Table 4: Different energies of Cu(111) k-points.

k-points	Energy (eV)
1,1,1	-86.866232
2,2,2	-75.221996
3,3,3	-76.169901
4,4,4	-75.800355
5,5,5	-75.946282
6,6,6	-75.837489

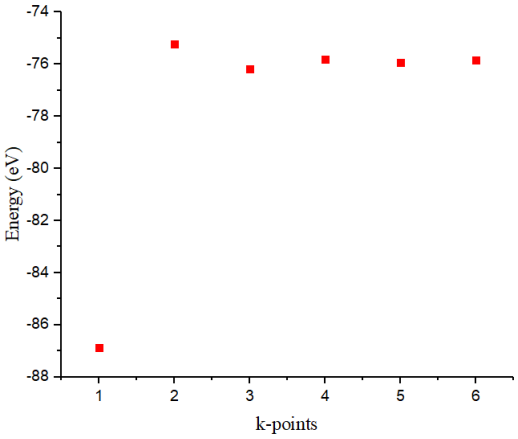

Figure 37: Evolution of energy by increasing the number of k-points.

The k-points (4,4,4) were decided to use in the Cu(111)-slab optimization because it is the first in the stable line of the k-point energies. The optimized Cu(111) unit cell and slab can be seen in Figure 38. The internal energy of the optimized copper slab was -302.5 eV.

When the k-points to graphene optimization were tested, the third k-point was kept as 1, as with the study by Vanin *et al.*[64]. The optimized energies are shown in Table 5 and the evolution of energies is seen in Figure 39. The optimized graphene surface was decided to be k-points (4,4,1) that had an energy of -33.9 eV. Optimized graphene unit cell and structure are shown in Figure 40.

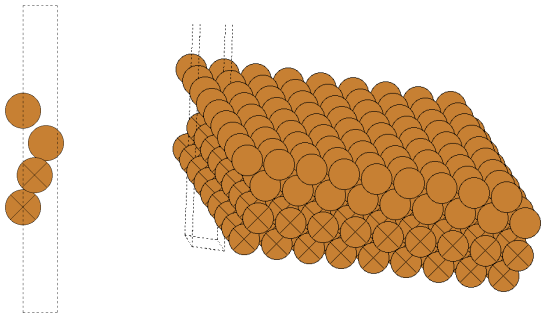

Figure 38: Optimized Cu unit cell (left) and slab (right).

Table 5: Different energies of graphene k-points.

k-points	Energy (eV)
1,1,1	-27.288324
2,2,1	-34.694438
3,3,1	-33.422045
4,4,1	-33.950779
5,5,1	-33.938089
6,6,1	-33.971665

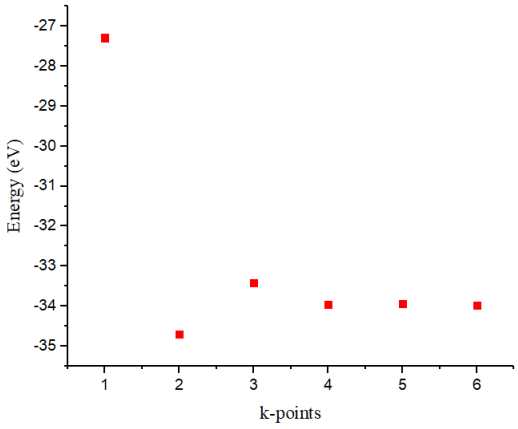

Figure 39: Evolution of energy of graphene by increasing the number of k-points.

The optimized graphene was added on top of the optimized Cu(111) with 2 bottom layers fixed and had an optimized energy of -336.05 eV. The distance between these two layers was 3.68 Å after optimization. This leads to the adhesion energy being 0.36 eV (equation 16). The optimized unit cell and structure are shown in Figure 41.

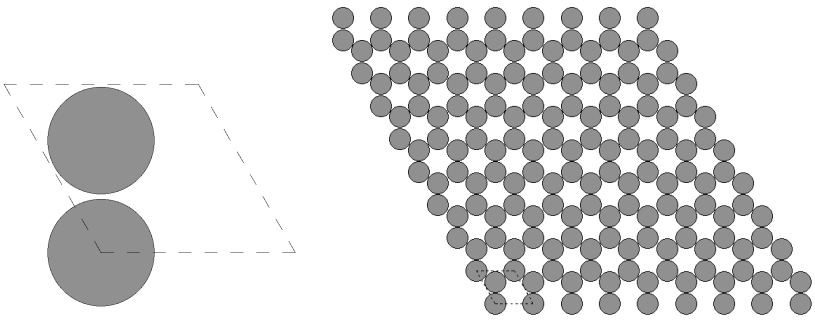

Figure 40: Optimized graphene unit cell (left) and full structure (right).

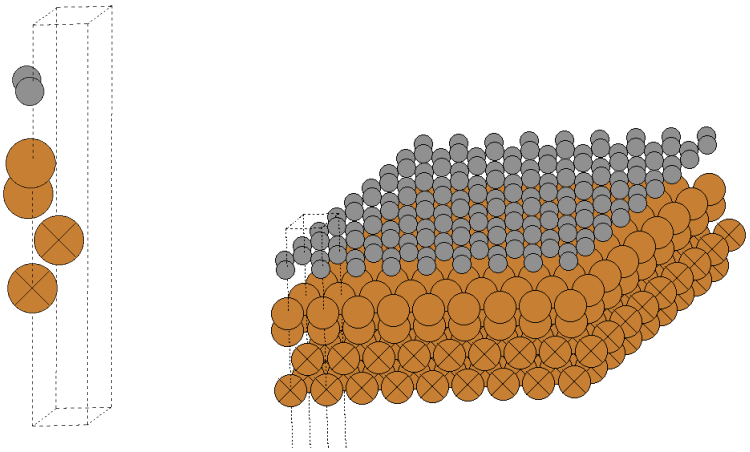

Figure 41: Graphene and copper layer combined unit cell (left) and structure (right).

The reported experimental adhesion energy between copper and graphene is 0.3-5.4 eV[34,35]. The computational value of 0.36 eV is in the reported range. However, the adhesion energy, extracted from the AFM data (section 7.5.1), was 0.4 μeV. This demonstrates the inaccuracy of the AFM data and its analysis.

10 Conclusion

Large-area graphene transfer was not achieved with the gels or methods used in this thesis. However, the research shows the presence of interactions between graphene and gel layer required for the transfer process.

The research in this thesis was performed to suggest an alternative approach to transfer graphene using soft gel materials. The literature reports the presence of graphene interactions with different gel materials while several graphene/gel applications have been

already assessed. Overall, three different gels were studied: HA gel, Fmoc-F gel, and the BocFFOtBu gel.

The HA gel is the most promising material as a potential transfer layer alternative since it withstood the etching conditions and transferred graphene. The transfer of graphene was confirmed by Raman spectroscopy. The size, however, of transferred graphene was small and could not be effectively used further. The findings when using HA gels suggest the development of graphene-HA gel interactions. The transfer process using HA films was also investigated, however, the results were negative as no graphene was transferred.

Future work can be focused on by testing the transfer process using different gel materials, to assess the optimal interactions with graphene-gel interactions which allow the transfer of graphene at a sufficient size. Another recommended approach is to assess a set of solvents for gelation and investigate potential solvent effects on the graphene's transfer process.

References

[1] Novoselov, K. S., Geim, A. K., Morozov, S. V., Jiang, D., Zhang, Y., Dubonos, S. V., Grigorieva, I. V. and Firsov, A. A., Electric Field Effect in Atomically Thin Carbon Films, *Science*, **2004**, *306*, 666–669.

[2] Avouris, P. and Dimitrakopoulos, C., Graphene: Synthesis and applications, *Materials Today*, **2012**, *15*, 86–97.

[3] Zhang, F., Li, Y. H., Li, J. Y., Tang, Z. R. and Xu, Y. J., 3D graphene-based gel photocatalysts for environmental pollutants degradation, *Environmental Pollution*, **2019**, *253*, 365–376.

[4] Miller, D. L., Keller, M. W., Shaw, J. M., Rice, K. P., Keller, R. R. and Diederichsen, K. M., Giant secondary grain growth in Cu films on sapphire, *AIP Advances*, **2013**, *3*, 0–10.

[5] Chen, M., Li, G., Li, W., Stekovic, D., Arkook, B., Itkis, M. E., Pekker, A., Bekyarova, E. and Haddon, R. C., Large-scale cellulose-assisted transfer of graphene toward industrial applications, *Carbon*, **2016**, *110*, 286–291.

[6] Seo, Y. M., Jang, W., Gu, T., Seok, H. J., Han, S., Choi, B. L., Kim, H. K., Chae, H., Kang, J. and Whang, D., Defect-Free Mechanical Graphene Transfer Using n-Doping Adhesive Gel Buffer, *ACS Nano*, **2021**, *15*, 11276–11284.

[7] Zhuang, B., Li, S., Li, S. and Yin, J., Ways to eliminate PMMA residues on graphene —— superclean graphene, *Carbon*, **2021**, *173*, 609–636.

[8] Zhang, Y., Wu, C. and Zhang, J., Interactions of graphene and graphene oxide with proteins and peptides, *Nanotechnology Reviews*, **2013**, *2*, 27–45.

[9] Abergel, D. S., Apalkov, V., Berashevich, J., Ziegler, K. and Chakraborty, T., Properties of graphene: A theoretical perspective, *Advances in Physics*, **2010**, *59*, 261–482.

[10] Wang, B., Si, L., Geng, J., Su, Y., Li, Y., Yan, X. and Chen, L., Controllable magnetic 3D nitrogen-doped graphene gel: Synthesis, characterization, and catalytic performance, *Applied Catalysis B: Environmental*, **2017**, *204*, 316–323.

[11] Chevigny, R., Schirmer, J., Piras, C. C., Johansson, A., Kalenius, E., Smith, D. K., Pettersson, M., Sitsanidis, E. D. and Nissinen, M., Triggering a transient organogelation system in a chemically active solvent, *Chemical Communications*, **2021**, *57*, 10375–10378.

[12] Gahane, A. Y., Singh, V., Kumar, A. and Kumar Thakur, A., Development of mechanism-based antibacterial synergy between Fmoc-phenylalanine hydrogel and aztreonam, *Biomaterials Science*, **2020**, *8*, 1996–2006.

[13] Collins, M. N. and Birkinshaw, C., Hyaluronic acid based scaffolds for tissue engineering - A review, *Carbohydrate Polymers*, **2013**, *92*, 1262–1279.

[14] Li, X. and Guo, J., Numerical investigation of the fracture properties of pre-cracked monocrystalline/polycrystalline graphene sheets, *Materials*, **2019**, *12*, DOI: 10.3390/ma12020263.

[15] Frank, I. W., Tanenbaum, D. M., Zande, A. M. van der and McEuen, P. L., Mechanical properties of suspended graphene sheets, *Journal of Vacuum Science Technology B: Microelectronics and Nanometer Structures*, **2007**, *25*, 2558.

[16] Tripathi, S. N., Saini, P., Gupta, D. and Choudhary, V., Electrical and mechanical properties of PMMA/reduced graphene oxide nanocomposites prepared via in situ polymerization, *Journal of Materials Science*, **2013**, *48*, 6223–6232.

[17] Carlsson, J. M., Hanke, F., Linic, S. and Scheffler, M., Two-Step Mechanism for Low-Temperature Oxidation of Vacancies in Graphene, *Physical Review Letters*, **2009**, *102*, 1–4.

[18] Johansson, A., Myllyperkiö, P., Koskinen, P., Aumanen, J., Koivistoinen, J., Tsai, H. C., Chen, C. H., Chang, L. Y., Hiltunen, V. M., Manninen, J. J., Woon, W. Y. and Pettersson, M., Optical Forging of Graphene into Three-Dimensional Shapes, *Nano Letters*, **2017**, *17*, 6469–6474.

[19] Wang, H., Wang, Y., Cao, X., Feng, M. and Lan, G., Vibrational properties of graphene and graphene layers, *Journal of Raman Spectroscopy*, **2009**, *40*, 1791–1796.

[20] Willock, D., *Molecular Symmetry*, John Wiley Sons Ltd., West Sussex, United kingdom, 2009, pp. 413.

[21] De Leon, A., Mellon, M., Mangadlao, J., Advincula, R. and Pentzer, E., The pH dependent reactions of graphene oxide with small molecule thiols, *RSC Advances*, **2018**, *8*, 18388–18395.

[22] Xu, T. and Sun, L., Structural defects in graphene, *Defects in Advanced Electronic Materials and Novel Low Dimensional Structures*, **2018**, *5*, 137–160.

[23] Ferrari, A. C. and Basko, D. M., Raman spectroscopy as a versatile tool for studying the properties of graphene, *Nature Nanotechnology*, **2013**, *8*, 235–246.

[24] Staveley, L., *The characterization of chemical purity organic compounds*, BUTTERWORTH Co., London, Britannia, 1971, pp. 149–153.

[25] J. Michael, H., *Modern Spectroscopy*. Wiley, 2004, vol. 4th ed, a) ss. 122–2.

[26] Strommen, D. P., Specific values of the depolarization ratio in raman spectroscopy: Their origins and significance, *Journal of Chemical Education*, **1986**, *63*, 803–807.

[27] Nanda, S. S., Kim, M. J., Yeom, K. S., An, S. S. A., Ju, H. and Yi, D. K., Raman spectrum of graphene with its versatile future perspectives, *TrAC - Trends in Analytical Chemistry*, **2016**, *80*, 125–131.

[28] Eaton, P. and West, P., *Atomic Force Microscopy*, 1st ed., Oxford University Press, New York, USA, 2010, a) pp. 2–8 b) 9–11 c) 22–23.

[29] Santos, N. C. and Castanho, M. A., An overview of the biophysical applications of atomic force microscopy, *Biophysical Chemistry*, **2004**, *107*, 133–149.

[30] Yu, G., Yan, X., Han, C. and Huang, F., Characterization of supramolecular gels, *Chemical Society Reviews*, **2013**, *42*, 6697–6722.

[31] Rao, K. V., Jayaramulu, K., Maji, T. K. and George, S. J., Supramolecular hydrogels and high-aspect-ratio nanofibers through charge-transfer-induced alternate coassembly, *Angewandte Chemie - International Edition*, **2010**, *49*, 4218–4222.

[32] Jones, R., Pollock, H. M., Cleaver, J. A. S. and Hodges, C. S., Adhesion Forces between Glass and Silicon Surfaces in Air Studied by AFM : Effects of Relative Humidity , Particle Size , Roughness , and Surface Treatment, **2002**, 8045–8055.

[33] Pocius, Dillard, D. A., Chaudhury, M., Chaudhury, M., Chaudhury, M. K., Dillard, D. A., Dillard, D. A., Pocius, Pocius, A. V., Pocius, A. V., Chaudhury, M., Pocius, A. and Dillard, D., *Adhesion Science and Engineering : Surfaces, Chemistry and Applications*, 1st ed., Elsevier Science Technology, New York, USA, 2002, vol. 2, a) pp. 76–80, b) pp. 195–211.

[34] Jiang, T. and Zhu, Y., microscopy with a microsphere tip †, **2015**, 10760–10766.

[35] Das, S., Lahiri, D., Lee, D.-y., Agarwal, A. and Choi, W., Measurements of the adhesion energy of graphene to metallic substrates, *Carbon*, **2013**, *59*, 121–129.

[36] Zong, Z., Chen, C. L., Dokmeci, M. R. and Wan, K. T., Direct measurement of graphene adhesion on silicon surface by intercalation of nanoparticles, *Journal of Applied Physics*, **2010**, *107*, 14–17.

[37] Babo, S., Ferreira, J. L., Ramos, A. M., Micheluz, A., Pamplona, M., Casimiro, M. H., Ferreira, L. M. and Melo, M. J., Characterization and long-term stability of historical PMMA: Impact of additives and acrylic sheet industrial production processes, *Polymers*, **2020**, *12*, DOI: 10.3390/POLYM12102198.

[38] Yasuda, H., Yamamoto, H. and Yokota, K., Synthesis of Monodispersed High Molecular Weight PoIy (MMA) Unit, *American chemical society*, **1992**, 4908–4910.

[39] Wan, A. M. D., Devadas, D. and Young, E. W. K., Sensors and Actuators B : Chemical Recycled polymethylmethacrylate (PMMA) microfluidic devices, *Sensors Actuators: B. Chemical*, **2017**, *253*, 738–744.

[40] Key Applications of Polymethyl Methacrylate (PMMA), Omnexus, 12/04/2021, https://omnexus.specialchem.com/selection-guide/polymethyl-methacrylate-pmma-acrylic-plastic/key-applications (visited on 07/28/2022).

[41] Du, X., Zhou, J., Shi, J. and Xu, B., Supramolecular Hydrogelators and Hydrogels: From Soft Matter to Molecular Biomaterials, *Chemical Reviews*, **2015**, *115*, 13165–13307.

[42] Moffat, J. R. and Smith, D. K., Controlled self-sorting in the assembly of 'multi-gelator' gels, *Chemical Communications*, **2009**, 316–318.

[43] Sangeetha, N. M. and Maitra, U., Supramolecular gels: Functions and uses, *Chemical Society Reviews*, **2005**, *34*, 821–836.

[44] Shapiro, Y. E., Structure and dynamics of hydrogels and organogels: An NMR spectroscopy approach, *Progress in Polymer Science (Oxford)*, **2011**, *36*, 1184–1253.

[45] An, Y., Solis, F. J. and Jiang, H., A thermodynamic model of physical gels, *Journal of the Mechanics and Physics of Solids*, **2010**, *58*, 2083–2099.

[46] Wang, Y., Tang, L. and Yu, J., Investigation on the assembled structure-property correlation of supramolecular hydrogel formed from low-molecular-weight gelator, *Journal of Colloid and Interface Science*, **2008**, *319*, 357–364.

[47] Zhou, B., Kang, W., Yang, H., Zhu, T., Zhang, H., Li, X., Sarsenbekuly, B. and Sarsenbek, T., Preparation and properties of an acid-resistant preformed particle gel for conformance control, *Journal of Petroleum Science and Engineering*, **2021**, *197*, 107964.

[48] González-Díaz, E. C. and Varghese, S., Hydrogels as extracellular matrix analogs, *Gels*, **2016**, *2*, DOI: 10.3390/gels2030020.

[49] Selyanin, M. A., Boykov, P. Y. and Khabarov, N. V., The History of Hyaluronic Acid, *Preparation, Properties, Application in Biology and Medicine*, **2015**, 1–8.

[50] Wu, H., Shi, H., Wang, Y., Jia, X., Tang, C., Zhang, J. and Yang, S., Hyaluronic acid conjugated graphene oxide for targeted drug delivery, *Carbon*, **2014**, *69*, 379–389.

[51] Alkrad, J. A., Mrestani, Y., Stroehl, D., Wartewig, S. and Neubert, R., Characterization of enzymatically digested hyaluronic acid using NMR, Raman, IR, and UV-Vis spectroscopies, *Journal of Pharmaceutical and Biomedical Analysis*, **2003**, *31*, 545–550.

[52] Jayawarna, V., Richardson, S. M., Hirst, A. R., Hodson, N. W., Saiani, A., Gough, J. E. and Ulijn, R. V., Introducing chemical functionality in Fmoc-peptide gels for cell culture, *Acta Biomaterialia*, **2009**, *5*, 934–943.

[53] Kang, J. and Yun, S. I., Fmoc-phenylalanine as a building block for hybrid double network hydrogels with enhanced mechanical properties, self-recovery, and shape memory capability, *Polymer*, **2022**, *255*, 125145.

[54] Gahane, A. Y., Ranjan, P., Singh, V., Sharma, R. K., Sinha, N., Sharma, M., Chaudhry, R. and Thakur, A. K., Fmoc-phenylalanine displays antibacterial activity against Gram-positive bacteria in gel and solution phases, *Soft Matter*, **2018**, *14*, 2234–2244.

[55] Singh, H., Gahane, A., Singh, V., Ghosh, S. and Thakur, A., Antibiofilm activity of Fmoc-phenylalanine against Gram-positive and Gram-negative bacterial biofilms, *Journal of Antibiotics*, **2021**, *74*, 407–416.

[56] Houlne, M. P., Sjostrom, C. M., Uibel, R. H., Kleimeyer, J. A. and Harris, J. M., Confocal Raman microscopy for monitoring chemical reactions on single optically trapped, solid-phase support particles, *Analytical Chemistry*, **2002**, *74*, 4311–4319.

[57] Lin, L. S., Lanza, T. J., E. de Laszlo, S., Truong, Q., Kamenecka, T. and Hagmann, W. K., Deprotection of N-tert-butoxycarbonyl (Boc) groups in the presence of tert-butyl esters, *Tetrahedron Letters*, **2000**, *41*, 7013–7016.

[58] Pattenaude, S. R., Streacker, L. M. and Ben-Amotz, D., Temperature and polarization dependent Raman spectra of liquid H2O and D2O, *Journal of Raman Spectroscopy*, **2018**, *49*, 1860–1866.

[59] Makela, M., Gordon, P., Tu, D., Soliman, C., Coté, G. L., Maitland, K. and Lin, P. T., Benzene Derivatives Analysis Using Aluminum Nitride Waveguide Raman Sensors, *Analytical Chemistry*, **2020**, *92*, 8917–8922.

[60] Lisesivdin, S. B. and Sarikavak-Lisesivdin, B., gpaw-tools – higher-level user interaction scripts for GPAW calculations and interatomic potential based structure optimization, *Computational Materials Science*, **2022**, *204*, 111201.

[61] Sellam, A., Heyd, R., Hlil, E. K., Koumina, A. and Hadaoui, A., Ab initio studies of the electronic structure induced by the CO and N2 adsorptions on graphene and on graphite slab, *Materials Today: Proceedings*, **2022**, *62*, 6287–6297.

[62] ASE-developers, Surfaces, ASE-developers, 07/04/2022, `https://wiki.fysik.dtu.dk/ase/ase/build/surface.html` (visited on 07/04/2022).

[63] Giovannetti, G., Khomyakov, P. A., Brocks, G., Karpan, V. M., Van Den Brink, J. and Kelly, P. J., Doping graphene with metal contacts, *Physical Review Letters*, **2008**, *101*, 4–7.

[64] Vanin, M., Mortensen, J. J., Kelkkanen, A. K., Garcia-Lastra, J. M., Thygesen, K. S. and Jacobsen, K. W., Graphene on metals: A Van Der Waals density functional study, *Physical Review B - Condensed Matter and Materials Physics*, **2010**, *81*, 1–4.

[65] Dion, M., Rydberg, H., Schröder, E., Langreth, D. C. and Lundqvist, B. I., Van der Waals density functional for general geometries, *Physical Review Letters*, **2004**, *92*, 22–25.

[66] Le, D., Kara, A., Schröder, E., Hyldgaard, P. and Rahman, T. S., Physisorption of nucleobases on graphene: A comparative van der Waals study, *Journal of Physics Condensed Matter*, **2012**, *24*, DOI: 10.1088/0953-8984/24/42/424210.